Available online at www.sciencedirect.com
ScienceDirect
Geochimica et Cosmochimica Acta 70 (2006) 4977–4996
Geochimica
www.elsevier.com/locate/gca

Oxygen isotopic studies of the interaction between xenoliths and mafic magma, Voisey's Bay Intrusion, Labrador, Canada

J. Mariga, E.M. Ripley *, C. Li

Department of Geological Sciences, Indiana University, Bloomington, IN 47405, USA

Received 6 December 2005; accepted in revised form 18 July 2006

Abstract

Sulfide mineralization in the Voisey's Bay Intrusion, Labrador, Canada, is closely associated with country rock xenoliths that have extensively reacted with basaltic magma. In order to better understand the processes that control the assimilation of country rocks by mafic magma, a detailed study of oxygen isotope systematics related to magma-country rock interaction in the Voisey's Bay area was undertaken. Protracted interaction of the xenoliths with magma produced refractory mineral assemblages in the xenoliths (2–10 cm in diameter) composed of Ca-rich plagioclase, corundum, hercynite, and minor magnetite. Overgrowth rims of plagioclase and biotite that surround most xenoliths separate the restites from the enclosing igneous matrix. The $\delta^{18}O$ values of minerals from regionally metamorphosed pelitic and quartzofeldspathic protoliths are: plagioclase (8.7–12.3‰), orthoclase (9.5–9.8‰), biotite (5.2–8.7‰), garnet (8.3–10.8‰), pyroxene (8.0–10.1‰), and quartz (9.6–14.0). The $\delta^{18}O$ values of minerals from the hornfels in the contact aureole of the intrusion are consistent with modeling which indicates that as a result of essentially closed system contact metamorphism oxygen isotope values should differ only slightly from those of the protoliths. Hercynite, plagioclase, and corundum separates from the xenoliths have $\delta^{18}O$ values that vary from 2.9‰ to 10.5‰, 5.6‰ to 10.9‰, and 2.0‰ to 6.8‰, respectively. Although a siliceous ^{18}O-enriched melt has been lost from the xenoliths, corundum, and feldspar $\delta^{18}O$ values are significantly lower than expected through melt loss alone. The relatively low $\delta^{18}O$ values of minerals from the xenoliths may be a function of incomplete isotopic exchange with surrounding mafic magma which had a $\delta^{18}O$ value of ~5.5‰ to 6.0‰. The high-^{18}O melt that was released from the xenoliths is partially recorded in the plagioclase overgrowth on the margin of the xenoliths ($\delta^{18}O$ values from 6.2‰ to 10.7‰), and in hercynite that replaced corundum. However, mass balance calculations indicate that a portion of the partial melt must have been transferred to magma that was moving through the conduit system. $\delta^{18}O$ and δD values of biotite surrounding the plagioclase overgrowth range from 5.0‰ to 6.2‰ and −58‰ to −80‰, respectively. These data suggest that the outermost rim associated with many xenoliths has closely approached isotopic equilibrium with uncontaminated mafic magma. The current gabbroic to troctolitic matrix of the xenoliths shows no evidence for contamination by the high-^{18}O partial melt from the xenoliths. The feldspar and biotite overgrowths on the xenoliths that formed after the motion of the xenoliths relative to the magma had stopped prevented further isotopic exchange between the xenoliths and final magma. The minerals within the xenoliths are not in oxygen isotopic equilibrium with each other, due in part to rapid thermal equilibration, partial melting, and partial exchange with flow through magma.

1. Introduction

The interaction of mantle-derived mafic magmas with crustal country rocks is a process that may be essential for the generation of many world-class Cu–Ni–PGE deposits (e.g., Naldrett, 1999). Previous studies have provided evidence for the attainment of sulfide saturation as a result of the addition of crustal sulfur to magma (e.g., Grinenko, 1985; Ripley, 1999). The contamination of mafic magma with siliceous country rocks can also lead to a decrease in the solubility of sulfur in the magma, and trigger the formation of an immiscible sulfide liquid (Irvine, 1975; Li and Naldrett, 1993; Li and Ripley, 2005).

* Corresponding author. Fax: +1 812 855 7961.
E-mail address: ripley@indiana.edu (E.M. Ripley).

0016-7037/$ - see front matter © 2006 Elsevier Inc. All rights reserved.
doi:10.1016/j.gca.2006.07.018

In the Voisey's Bay Ni–Cu–Co deposit in Labrador, Canada, abundant xenoliths of country rocks are found in close association with sulfide mineralization, and provide petrological evidence for the link between magma contamination and ore formation. Xenoliths can often be utilized to evaluate the poorly understood mechanisms of mass transfer between magmas and country rock. In dynamic magma conduit systems, where large amounts of magma may have passed through the conduit-magma chamber network, little or no evidence of the assimilation process may remain in the igneous rock. For this reason an understanding of the evolution of the country rock xenoliths is essential.

Because of the large differences that may exist between the oxygen isotopic compositions of metasedimentary rock types and mafic magma, oxygen isotopic values can be sensitive indicators of magma contamination. At the Voisey's Bay deposit, earlier studies of the intrusive rocks showed little or no oxygen isotopic evidence of contamination, even though the xenoliths are in many cases refractory and suggest a prolonged history of interaction with magma (Ripley et al., 1999, 2000). As part of a detailed investigation of contamination processes that occurred in the Voisey's Bay Intrusion, we initiated a study of the oxygen isotopic systematics of gneissic country rocks, contact hornfels, xenoliths, and igneous matrix surrounding the xenoliths. The objectives of this study were to quantify the oxygen isotopic fractionation that accompanied mineral transformations in the xenoliths and to utilize the isotopic variations to better understand the mechanisms of magma-country rock interaction. Hydrogen isotopic measurements of biotite were also undertaken to better evaluate the role of fluid in magma–xenolith interaction.

2. Geological background

2.1. Regional and local geology

The Voisey's Bay Ni–Cu–Co sulfide deposit is located in Northern Labrador, Canada, approximately 30 km southwest of the town of Nain (Fig. 1). Details of the geology of the Nain area have been given by several authors (e.g., Berg and Docka, 1983; Wardle, 1983; Lee, 1987; Wardle et al., 1990a,b; Ryan et al., 1995; Ryan, 2000; McFarlane et al., 2003). A brief description of regional and local geology is presented here. The Voisey's Bay deposit occurs near

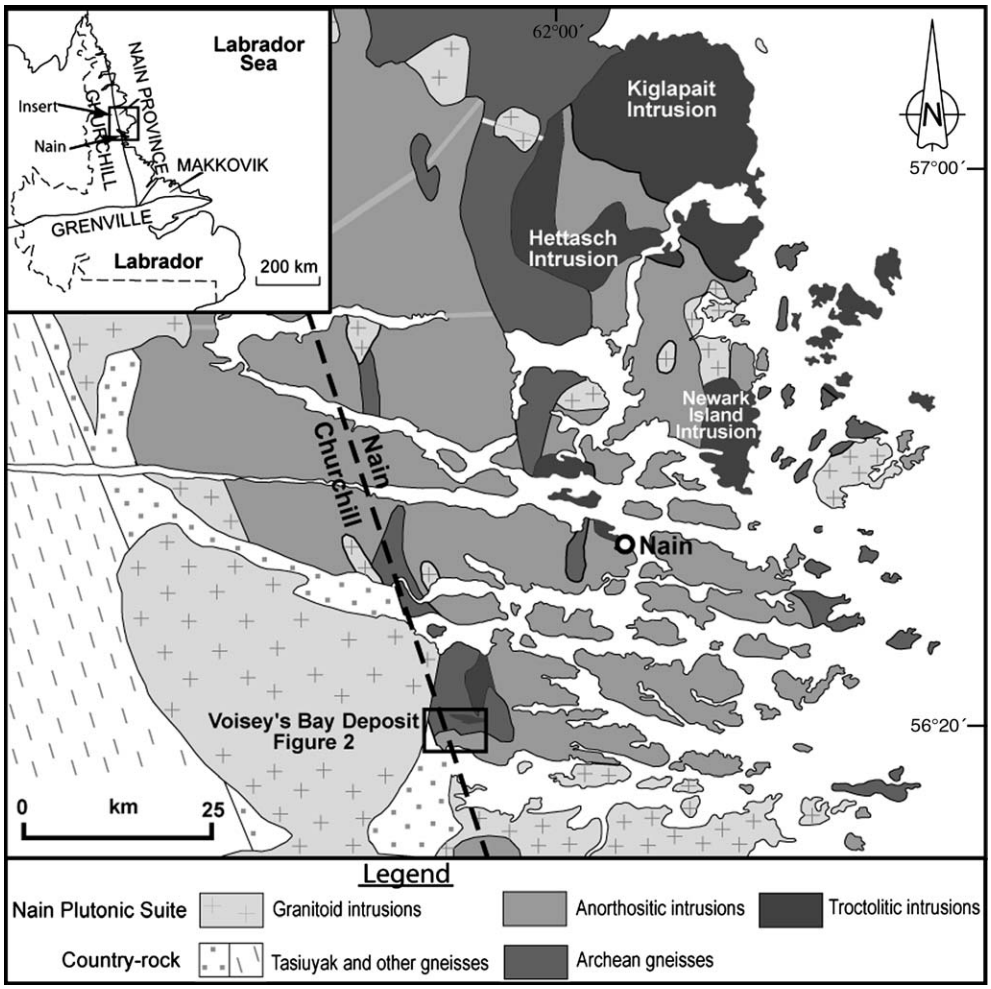

Fig. 1. Regional geology of the area around the Voisey's Bay deposit (adapted from Ryan et al., 1995).

the contact of two lithotectonic units called the Nain and the Churchill provinces (Fig. 1). The collision of the two lithotectonic provinces took place during the 1.86–1.82 Ga Torngat orogeny. The Voisey's Bay deposit is hosted by a troctolitic intrusion that belongs to the Nain Plutonic Suite. The Nain Plutonic Suite consists of granitic, anorthositic, and troctolitic intrusions that formed at 1.35–1.30 Ga (Hamilton et al., 1994; Amelin et al., 1999). Rocks of the Proterozoic Churchill province include a supracrustal sequence of interbanded garnet-sillimanite-bearing, sulfidic, and graphitic quartzofeldspathic metasedimentary lithologies referred to as the Tasiuyak Gneiss, minor quartzofeldspathic orthogneisses of Archean age, and enderbitic orthogneisses. Rocks of the Archean Nain province are granitic, intermediate and mafic orthogneisses.

The Voisey's Bay Intrusion consists of the Reid Brook subchamber to the west, the Eastern Deeps subchamber to the east, and a feeder dike connecting them (Fig. 2). The Tasiuyak Gneiss is present in the Western portion of the deposit and the enderbitic and quartzofeldspathic gneisses are present further to the east (see Fig. 2). Various types of texturally distinct rocks such as olivine gabbro, leucotroctolite, feeder gabbro, normal troctolite, varied-textured troctolite, leopard troctolite, ferrodiorite, and the basal breccia or feeder breccia are present in different parts of the Voisey's Bay Intrusion (Naldrett et al., 1996; Li and Naldrett, 1999; Li and Naldrett, 2000; Fig. 3). Its geology and petrography have been reported by Ryan et al. (1995), Naldrett et al. (1996), and Li and Naldrett (1999). From east to west, different sulfide ore zones in the intrusion are the Eastern Deeps, Ovoid, Mini Ovoid, Discovery Hill, and the Reid Brook (Evans-Lamswood et al., 2000; Fig. 2).

2.2. Mineralogical and textural characteristics of country rocks and xenoliths

The Tasiuyak Gneiss exhibits compositional banding with leucosomes consisting of plagioclase (~40%), ribbon textured quartz (10–30%) and K-feldspar (10–20%), and melanosomes consisting of biotite(15%), poikilitic garnet porphyroblasts (15–20%), pyroxene (15–20%), and plagioclase (10–20%). Zones with up to 60% quartz are also locally present. Magnetite, pyrrhotite, sillimanite, and graphite are generally minor, but layers that contain up to 30% graphite and 10% pyrrhotite are observed in places. Archean quartzofeldspathic gneisses consist of plagioclase (10–30%), K-feldspar (10–25%), quartz (20–35%), biotite (~5%), and minor hornblende. Mafic gneisses of the Nain province consist of biotite (10–15%), plagioclase (30–40%), amphibole (~10–20%), and clinopyroxene (~20%). The enderbitic gneiss is composed of plagioclase (~40%), clinopyroxene (10–15%), orthopyroxene (10–15%), amphibole (5–10%), biotite (5%), and quartz (up to15%). Pyroxene and biotite both have amphibole coronae. Weak preferential alignment of biotite, amphibole, and pyroxene defines a gneissic texture.

Xenoliths of country rocks that range in size from 2 to 10 cm in their long dimension occur predominantly in the base of the Eastern Deeps subchamber (Basal Breccia) and within the Feeder Dike (Feeder Breccia) (see Fig. 3). Volume ratios of xenoliths to igneous matrix are variable, but locally reach values as high as one. The xenoliths are divided into five types: light-cored, dark-cored, laminated, massive, and variegated. Light-cored xenoliths are characterized by a distinct pink to

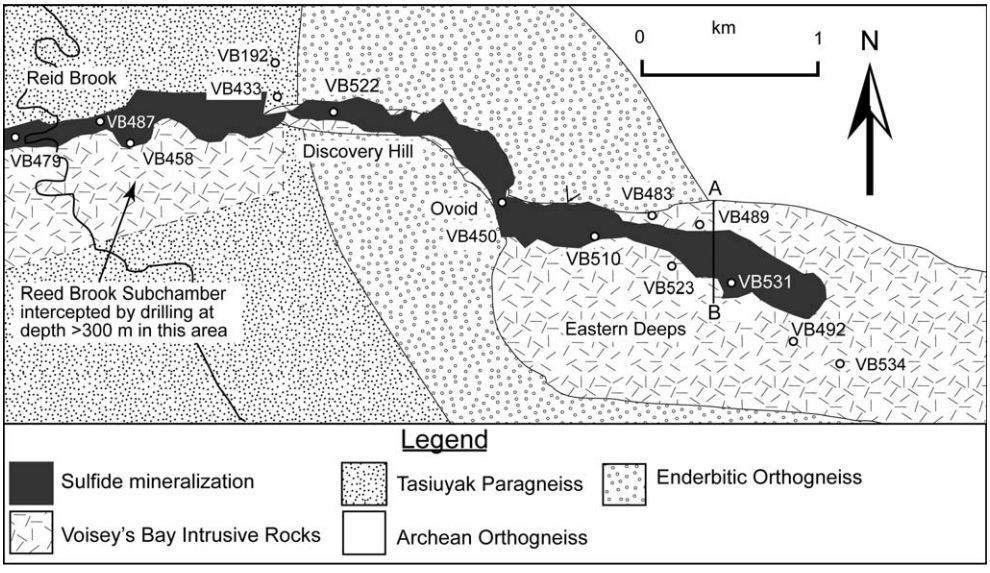

Fig. 2. Plan view of the Voisey's Bay Intrusion showing different sections of the deposit and the locations of sampled drill cores. Samples with prefix TG were collected about 2 km south of the mapped area. Sulfide mineralization has been projected to the surface and shown here in black. Also note the changes in the immediate country rocks along the strike of the intrusion. Line (A and B) represents the profile shown in Fig. 3 (adapted from Li and Naldrett, 2000).

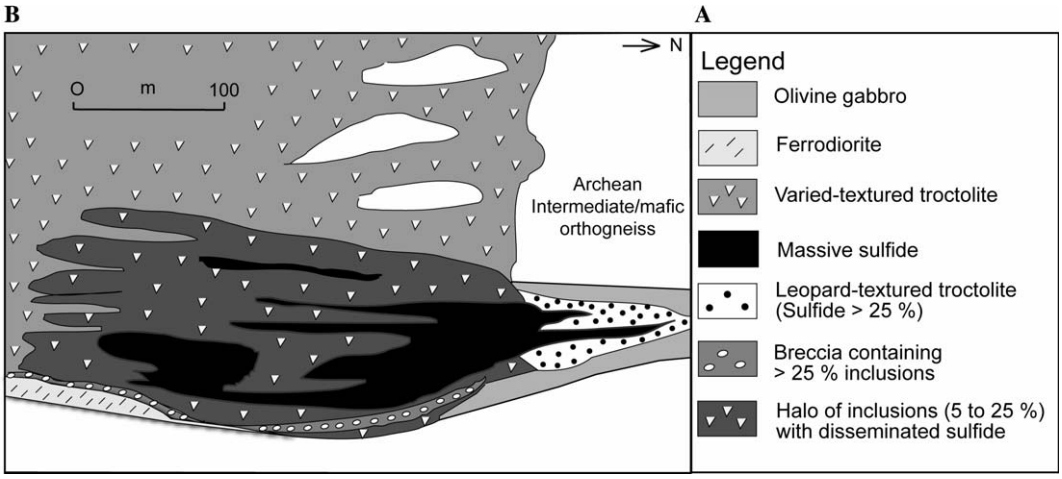

Fig. 3. Simplified stratigraphic cross section through the lower part of the Eastern Deeps Subchamber showing the mineralized zone at Voisey's Bay and the position of the Basal Breccia Sequence. No vertical exaggeration.

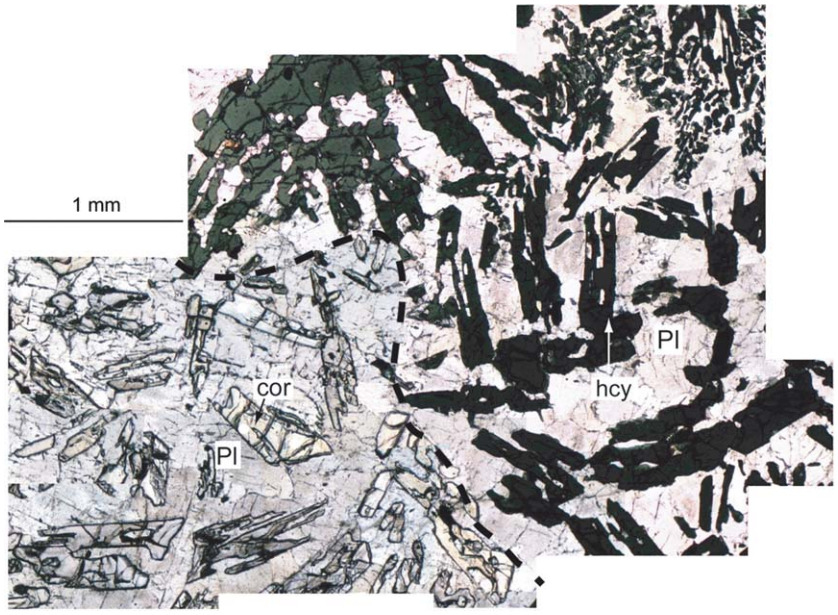

Fig. 4. Composite photomicrograph of a light-cored xenolith illustrating a relatively sharp contact between a plagioclase (pl)—corundum (cor) core and a hercynite (hcy)—plagioclase rim. The acicular hercynite is thought to be a replacement of corundum. (For interpretation of the references to color in this figure legend, the reader is referred to the web version of this paper.)

beige (plagioclase + corundum) core mantled by a dark-green band rich in hercynite (Fig. 4), a conspicuous rim of white plagioclase (up to ~0.5 cm) and an outer biotite-rich band. Some grains of corundum are replaced by hercynite (Fig. 4).

Dark-cored xenoliths consist of a dark-green hercynite-rich core, a 1–3 mm white plagioclase overgrowth rim, and an outer biotite-rich band. Massive xenoliths are relatively small (<5 cm in length) and are similar to dark-cored xenoliths except for the lack of plagioclase overgrowth and a biotite rim. Massive xenoliths consist of hercynite with various textures and minor magnetite and Ca-rich plagioclase. These types of xenoliths are almost always associated with massive sulfides. Laminated xenoliths are characterized by dark-green hercynite-rich bands that alternate with plagioclase-rich bands. Variegated xenoliths have a motley appearance, which is defined by patches of contrasting colors; dark-green hercynite patches are mixed with pink to beige plagioclase- and corundum-rich patches. Variegated xenoliths are commonly surrounded by a biotite-rich band.

Generally, all of the xenoliths from the Voisey's Bay Intrusion have similar restite mineral assemblages consisting of hercynite, Ca-rich plagioclase, and magnetite. Corundum is present only in the cores of light-cored xenoliths. Three textural varieties of hercynite, acicular, bulbous, and granular, are observed in the xenoliths. These shapes mimic corundum, garnet, and hypersthene, respectively. Mineral banding and vermicular symplectitic textures that commonly occur in the hornfels are also present in some of the xenoliths.

2.3. Origin of the restite assemblages

The refractory mineral phases (hercynite, magnetite, Ca-rich plagioclase, and corundum), in the xenoliths of the Voisey's Bay Intrusion formed soon after the xenoliths were immersed in magma. It can be readily shown (e.g., Carslaw and Jaeger, 1986) that xenoliths in the Voisey's Bay Intrusion would have achieved thermal equilibrium with the enclosing magma at temperatures greater than 1150 °C in less than a few days. Mariga et al. (2006) have proposed that the refractory mineral assemblages formed via partial melting as magma flowed through the conduit system. Pseudomorphic textures of hercynite after various precursors such as corundum, pyroxene, and garnet indicate that the xenoliths maintained their morphologies during the removal of partial melt. Mariga et al. (2006) interpret both textural and chemical data as indicating that as reaction with magma progressed, corundum in the xenoliths was converted to hercynite by obtaining FeO and MgO from the magma (Fig. 5). As the reaction front moved inward the xenoliths were converted to dark-cored xenoliths, and finally to massive xenoliths. Density differences between partial melt (~2.6 g/cc), remnant minerals (corundum, 3.4 g/cc; hercynite, ~4.4 g/cc), and mafic magma aided the separation of partial melt from the restite. We cannot rule out the possibility that xenoliths in the Voisey's Bay Intrusion have been derived from multiple protoliths, and perhaps from distant sources. However, in at least the Reid Brook zone the presence of hercynite with bulbous and vermicular textures that are similar to the textures observed in the immediate Tasiuyak Gneiss country rock suggest that the xenoliths were locally derived.

3. Previous isotopic studies of the Voisey's Bay Intrusion and country rocks

Radiogenic and stable isotope studies of the Voisey's Bay Intrusion and the immediate country rocks have been conducted to understand age and petrogenetic relationships (Amelin et al., 1999, 2000). The Nd, Sr, and Pb isotopic data indicate that the parental magmas of the Voisey's Bay Intrusion were either derived from an enriched lithospheric mantle or contaminated by about 8–13% of Tasiuyak Gneiss. Despite anomalous Nd, Sr, and Pb isotopic values, samples from the Voisey's Bay Intrusion exhibit isotopic homogeneity. The Re–Os isotopic studies of Lambert et al. (1999, 2000) confirmed the presence of crustal osmium in the intrusive rocks. Sulfide and oxide mineral separates defined a precise isochron (1004 ± 20 Ma), albeit younger than that defined by bulk whole rock samples (1320 Ma). Lambert et al. (2000) concluded that the deviation between sulfide separates and bulk rock isochrons was indicative of resetting of the Re–Os system at a mineral grain scale. Sulfide samples are characterized by high γ_{Os} values which were interpreted to be indicative of extensive crustal contamination.

Sulfur isotopic values of mineralized samples from the Voisey's Bay Intrusion range between 0.0‰ and −4.0‰

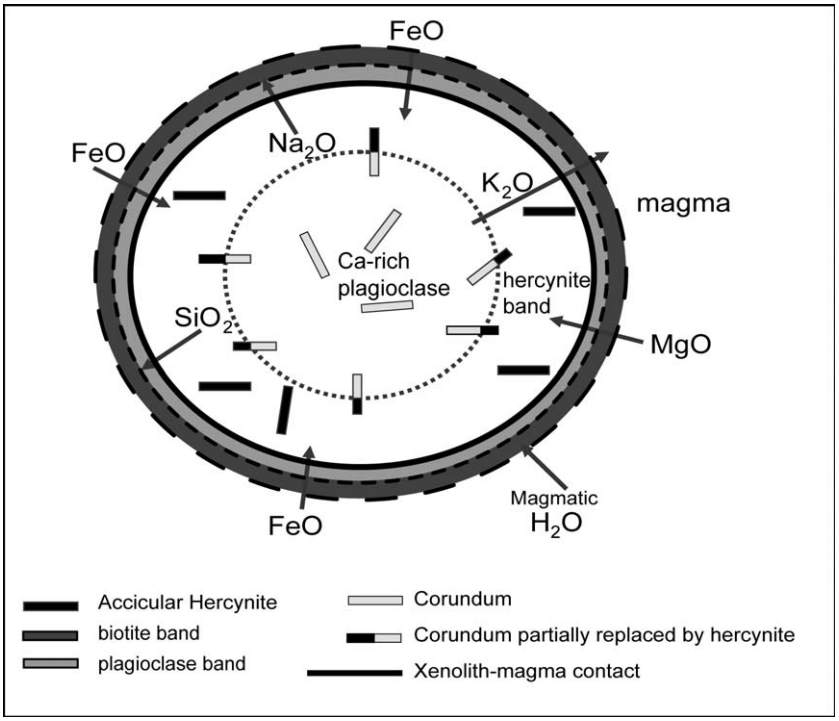

Fig. 5. Schematic diagram illustrating mineral zoning found in xenoliths within the Voisey's Bay Intrusion, and direction of mass transfer (modified from Mariga et al., 2006). The replaced ends of corundum always point away from the center of the xenolith. A sharp replacement front separates xenolith cores with unreplaced corundum from rims with no corundum but acicular hercynite. Bands of plagioclase and biotite enclose most xenoliths.

(Ripley et al., 1999, 2002). Samples from the Reid Brook zone have more negative $\delta^{34}S$ values than those from the Eastern Deeps, the Ovoid, and the Discovery Hill zone. Sulfide minerals in the Tasiuyak Gneiss have $\delta^{34}S$ values between −17.0‰ and +18.3‰, with an average similar to that of the Voisey's Bay Intrusion. On the basis of low sulfide concentrations, Ripley et al. (2002) ruled out the enderbitic and Archean orthogneisses as potential sulfur contaminants, and suggested that the most likely source was the Tasiuyak Gneiss.

Well-crystallized graphite from the Voisey's Bay Intrusion is characterized by $\delta^{13}C$ values between −18.3‰ and −24.8‰ (Ripley et al., 2002) that differ only slightly from those of the Tasiuyak Gneiss (−13.1‰ to −31.7‰). Ripley et al. (2002) interpreted the carbon isotope similarity between the igneous rocks and the Tasiuyak Gneiss as evidence for assimilation of the later.

Ripley et al. (1999, 2000) reported the presence of anomalously high $\delta^{18}O$ values within ~2 cm of the margin of country rock xenoliths, but found no anomalous isotopic signatures in the rocks further from the xenoliths. Ripley et al. (1999, 2000) attributed the elevated $\delta^{18}O$ values around the xenoliths to late stage diffusive exchange, and the lack of elevated $\delta^{18}O$ values away from the diffusive boundary layer to the dynamic nature of continuous magma flow that removed the early partial melt from the xenoliths.

4. Sampling and analytical methods

Samples for this study were mostly collected from drill cores, with a few collected from outcrop (Fig. 2). Xenolith samples were examined using standard transmitted and reflected light microscopy. Mineral grains for oxygen isotopic analyses were separated from the country rocks, hornfels, and xenoliths using a 0.5 mm diamond-tipped drill bit. Fine-grained minerals were drilled under a binocular microscope. Collected powder was less than 100-mesh. Corundum was separated by pulverizing the samples (<1 mm) and reacting with hydrofluoric acid for a period of approximately two weeks. The samples were thoroughly cleaned with nitric acid, and rinsed with deionized water before being dried in a vacuum oven at 200 °C for a period of more that 24 h. Corundum was crushed to less than 100-mesh prior to oxygen extraction.

Silicate and oxide minerals were reacted with BrF_5 in nickel vessels to liberate oxygen following the method of Clayton and Mayeda (1963). Garnet and corundum were reacted at temperatures between 650 and 690 °C, whereas other minerals were treated at 600 °C. Oxygen yields for garnet, as well as hercynite, ranged from 90% to 100%. Corundum is a particularly refractory mineral and yields for samples varied from 70% to 90%. Oxygen was converted to carbon dioxide by reaction with a hot graphite disk. Oxygen isotope analyses were performed using a Finnigan MAT 252 stable isotope ratio mass spectrometer and results were reported using the standard δ-notation relative to V-SMOW. Analytical uncertainty of isotopic measurements was ~0.05‰, and sample reproducibility was within ±0.25‰ for all minerals. Duplicate and triplicate analyses of corundum samples showed no variation of $\delta^{18}O$ values with yield. The range of $\delta^{18}O$ values for corundum separates is identical to the range for *in situ* measurements of corundum determined by ion microprobe analyses. The NBS-28 quartz standard has a value of 9.6 ± 0.2‰ in our lab; an internal laser ruby standard is characterized by a value of 15.7 ± 0.2‰.

Samples for hydrogen isotopic analyses were analyzed using a high-temperature-elemental analyzer-continuous flow method similar to that reported by Sharp et al. (2001). Samples were loaded into silver cups and combusted at 1400 °C in a glassy carbon column. Hydrogen was analyzed using a Finnigan Delta Plus-XP stable isotope mass spectrometer. Several standards were run with each series of analyses. Internal standards included kaolinite (−65‰), muscovite (−74‰), actinolite (−69‰), and two serpentines (−66‰ and −100‰), all calibrated relative to an NBS-30 biotite value of −65‰. Results are reported in delta notation with respect to VSMOW. Instrumental reproducibility was within ±0.2‰ and sample reproducibility was ±2‰.

5. Results

5.1. Oxygen isotopic composition of country rocks, contact metamorphosed hornfels, xenoliths, and igneous matrix

Results of oxygen isotope analyses of mineral separates from regional and contact aureole assemblages of various country rocks in the area of the Voisey's Bay Intrusion are shown in Table 1 and Fig. 6. Of note are the following: (1) $\delta^{18}O$ values of garnet, pyroxene, quartz, and plagioclase from the Tasiuyak Gneiss and its hornfels are similar. (2) Minerals from the enderbitic and mafic gneisses have lower $\delta^{18}O$ values than those from the Tasiuyak Gneiss. (3) Quartz and feldspar from the Archean quartzofeldspathic gneiss have $\delta^{18}O$ values that range between 9.0 and 10.7‰. (4) Biotite in all rock types is characterized by the lowest $\delta^{18}O$ values, with mean values of 6.8‰ in the Tasiuyak Gneiss and 5.8‰ in the enderbitic gneiss. δD values of biotite from Tasiuyak Gneiss hornfels range between −56‰ and −58‰.

$\delta^{18}O$ values of plagioclase, corundum, and hercynite from the xenoliths, plagioclase, and biotite from the overgrowth bands, and plagioclase from the enclosing igneous matrix are given in Table 2 and Fig. 7. Average values of hercynite, corundum, Ca-rich (An_{50-80}) plagioclase in the xenoliths, and plagioclase (An_{45-60}) from the overgrowth bands that surround the xenoliths are 6.6‰, 5.1‰, 8.8‰, and 7.6‰, respectively. $\delta^{18}O$ and δD values of the biotite-rich bands are given in Table 3. Average biotite $\delta^{18}O$ and δD values are 5.6‰ and −71‰, respectively.

Figs. 8–10 illustrate several representative oxygen isotope profiles across the xenoliths from the Voisey's Bay

Table 1
Oxygen isotope values of minerals from country rocks

Sample No.	Depth	Type of sample	Rock type	Mineral	$\delta^{18}O$ (‰ VSMOW)
VB192	252.7	Aureole	Endebitic gneiss	Biotite	5.2
VB264	104.2	Regional	Endebitic gneiss	Biotite	6.3
VB192	243	Aureole	Endebitic gneiss	Plagioclase	7.2
VB192	252.7	Aureole	Endebitic gneiss	Plagioclase	7.7
VB264	104.2	Regional	Endebitic gneiss	Plagioclase	6.8
VB264	104.2	Regional	Endebitic gneiss	Plagioclase	7.2
VB192	64.2	Regional	Endebitic gneiss	Plagioclase	7.6
VB264	104.2	Regional	Endebitic gneiss	Plagioclase	7.9
VB192	252.7	Aureole	Endebitic gneiss	Pyroxene	5.7
VB264	104.2	Regional	Endebitic gneiss	Pyroxene	6.2
VB264	104.2	Regional	Endebitic gneiss	Pyroxene	6.9
VB192	243	Aureole	Endebitic gneiss	Pyroxene/amphibole	7.5
VB192	252.7	Aureole	Endebitic gneiss	Quartz	7.1
VB264	104.2	Regional	Endebitic gneiss	Quartz	7.8
AG	Outcrop	Regional	Nain gneiss	Biotite	5.2
AG	Outcrop	Regional	Nain gneiss	Orthoclase	9.8
AG	Outcrop	Regional	Nain gneiss	Melanosome	5.3
AG	Outcrop	Regional	Nain gneiss	Melanosome	7.8
AG	Outcrop	Regional	Nain gneiss	Orthoclase	9.5
AG	Outcrop	Regional	Nain gneiss	Plagioclase	9.0
AG	Outcrop	Regional	Nain gneiss	Plagioclase	10.7
AG	Outcrop	Regional	Nain gneiss	Quartz	9.6
AG	Outcrop	Regional	Nain gneiss	Quartz	10.5
AG	Outcrop	Regional	Nain gneiss	Quartz	10.7
S1	Outcrop	Regional	Nain mafic gneiss	Biotite	5.8
S1	Outcrop	Regional	Nain mafic gneiss	Plagioclase	6.8
S1	Outcrop	Regional	Nain mafic gneiss	Plagioclase	7.1
S1	Outcrop	Regional	Nain mafic gneiss	Pyroxene	6.1
S1	Outcrop	Regional	Nain mafic gneiss	Pyroxene	6.3
VB192	293	Aureole	Tasiuyak Gneiss	Biotite	6.7
VB192	293	Aureole	Tasiuyak Gneiss	Biotite	7.0
VB487	581.5	Aureole	Tasiuyak Gneiss	Biotite	5.2
VB487	407.5	Aureole	Tasiuyak Gneiss	Biotite	6.3
VB433	115	Regional	Tasiuyak Gneiss	Biotite	8.7
VB192	293	Aureole	Tasiuyak Gneiss	Garnet	8.5
VB192	293	Aureole	Tasiuyak Gneiss	Garnet	8.8
VB487	407.5	Aureole	Tasiuyak Gneiss	Garnet	8.9
VB433	152	Aureole	Tasiuyak Gneiss	Garnet	9.1
VB487	581.5	Aureole	Tasiuyak Gneiss	Garnet	9.2
VB433	118	Aureole	Tasiuyak Gneiss	Garnet	9.8
VB487	361	Aureole	Tasiuyak Gneiss	Garnet	10.1
VB433	119.5	Aureole	Tasiuyak Gneiss	Garnet	10.2
VB487	361	Aureole	Tasiuyak Gneiss	Garnet	10.3
VB487	407.5	Aureole	Tasiuyak Gneiss	Garnet	10.4
VB433	152	Aureole	Tasiuyak Gneiss	Garnet	10.7
VB433	107	Regional	Tasiuyak Gneiss	Garnet	8.3
VB433	115	Regional	Tasiuyak Gneiss	Garnet	9.0
TG2	Outcrop	Regional	Tasiuyak Gneiss	Garnet	9.1
TG3	Outcrop	Regional	Tasiuyak Gneiss	Garnet	9.6
TG1	Outcrop	Regional	Tasiuyak Gneiss	Garnet	10.0
VB433	107	Regional	Tasiuyak Gneiss	Garnet	10.8
VB433	112	Regional	Tasiuyak Gneiss	Hercynite	6.3
VB433	112	Regional	Tasiuyak Gneiss	Hercynite	7.1
VB192	293	Aureole	Tasiuyak Gneiss	Plagioclase	9.6
VB192	293	Aureole	Tasiuyak Gneiss	Plagioclase	10.9
VB433	152	Aureole	Tasiuyak Gneiss	Plagioclase	10.0
VB433	118	Aureole	Tasiuyak Gneiss	Plagioclase	10.5
VB433	119.5	Aureole	Tasiuyak Gneiss	Plagioclase	10.5
VB487	407.5	Aureole	Tasiuyak Gneiss	Plagioclase	10.7
VB487	581.5	Aureole	Tasiuyak Gneiss	Plagioclase	11.8
VB433	112	Regional	Tasiuyak Gneiss	Plagioclase	8.7
VB433	107	Regional	Tasiuyak Gneiss	Plagioclase	10.9
VB433	115	Regional	Tasiuyak Gneiss	Plagioclase	11.5
TG2	Outcrop	Regional	Tasiuyak Gneiss	Plagioclase	11.6

(*continued on next page*)

Table 1 (*continued*)

Sample No.	Depth	Type of sample	Rock type	Mineral	δ^{18}O (‰ VSMOW)
VB433	109	Regional	Tasiuyak Gneiss	Plagioclase	11.8
TG3	Outcrop	Regional	Tasiuyak Gneiss	Plagioclase	11.9
TG1	Outcrop	Regional	Tasiuyak Gneiss	Plagioclase	12.0
VB433	107	regional	Tasiuyak Gneiss	Plagioclase	12.3
VB192	293	Aureole	Tasiuyak Gneiss	Pyroxene	8.8
VB487	581.5	Aureole	Tasiuyak Gneiss	Pyroxene	8.3
VB487	407.5	Aureole	Tasiuyak Gneiss	Pyroxene	9.3
VB487	407.5	Aureole	Tasiuyak Gneiss	Pyroxene	9.6
VB433	119.5	Aureole	Tasiuyak Gneiss	Pyroxene	10.1
VB433	109	Regional	Tasiuyak Gneiss	Pyroxene	8.0
VB433	115	Regional	Tasiuyak Gneiss	Pyroxene	9.0
TG2	Outcrop	Regional	Tasiuyak Gneiss	Pyroxene	9.1
VB433	109	Regional	Tasiuyak Gneiss	Pyroxene	9.3
TG3	Outcrop	Regional	Tasiuyak Gneiss	Pyroxene	9.4
TG1	Outcrop	Regional	Tasiuyak Gneiss	Pyroxene	9.6
VB192	293	Aureole	Tasiuyak Gneiss	Quartz	12.1
VB433	119.5	Aureole	Tasiuyak Gneiss	Quartz	10.4
VB433	118	Aureole	Tasiuyak Gneiss	Quartz	12.2
VB487	407.5	Aureole	Tasiuyak Gneiss	Quartz	12.8
VB487	581.5	Aureole	Tasiuyak Gneiss	Quartz	13.5
VB487	581.5	Aureole	Tasiuyak Gneiss	Quartz	14.0
VB433	115	Regional	Tasiuyak Gneiss	Quartz	12.1
TG2	Outcrop	Regional	Tasiuyak Gneiss	Quartz	12.7
VB433	109	Regional	Tasiuyak Gneiss	Quartz	13.0
TG3	Outcrop	Regional	Tasiuyak Gneiss	Quartz	13.0
TG1	Outcrop	Regional	Tasiuyak Gneiss	Quartz	13.5

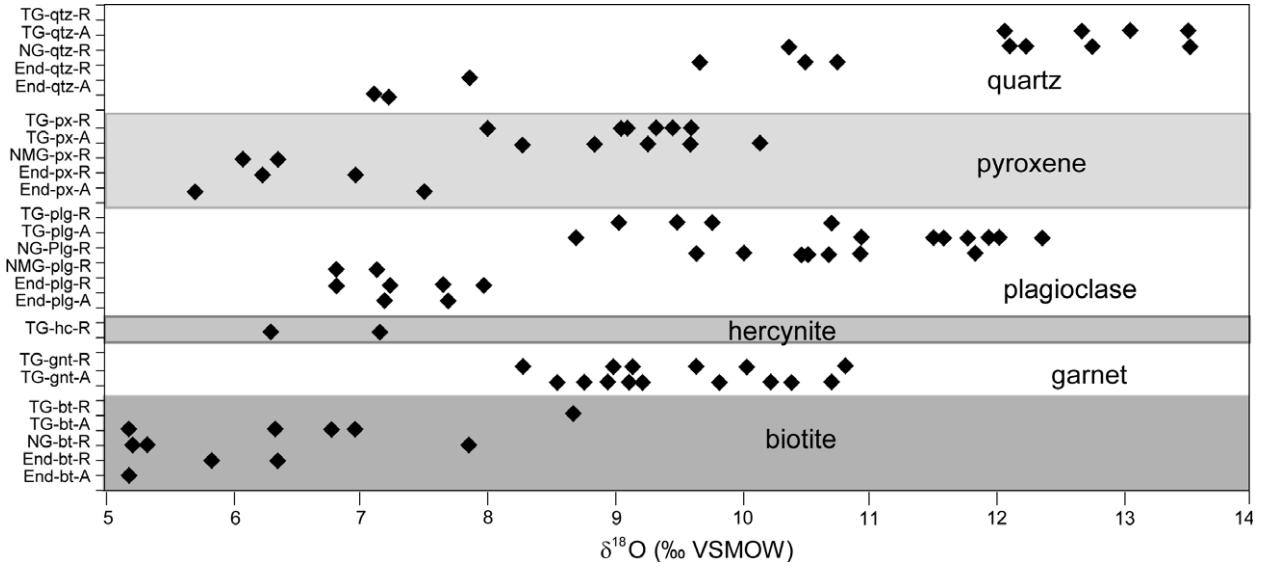

Fig. 6. Ranges of δ^{18}O values of biotite (bt), plagioclase (plg), hercynite (hc), pyroxene (px), garnet (gnt), and quartz (qtz) separates from both regional (R), and contact aureole (A) assemblages of the enderbitic gneiss (End), quartzofeldspathic gneiss (NG), Tasiuyak Gneiss (TG), and the Nain Mafic gneiss (NMG).

Intrusion. Mixtures of corundum and plagioclase that constitute the cores of light-cored xenoliths are characterized by values from 4‰ to 10.5‰ that primarily reflect variations in the modal proportions of corundum and plagioclase. Hercynite in dark-cored and massive xenoliths ranges from 5.7‰ to 10.3‰, with only two values in excess of 6.9‰. Plagioclase in the cores of dark-cored xenoliths may have δ^{18}O values that are higher or lower than those of plagioclase in the overgrowth bands.

6. Discussion

6.1. δ^{18}O variations in the regional and contact metamorphic assemblages and isotopic thermometry

The δ^{18}O values of leucosomes and melanosomes of the Tasiuyak Gneiss are different. Leucosomes consisting of plagioclase, K-feldspar, and quartz yield relatively high bulk δ^{18}O values (9.8–14.0‰) compared to melanosomes

Table 2
$\delta^{18}O$ values of minerals from xenoliths, overgrowth bands, and enclosing igneous matrix

Core No.	Depth	Environment	Type of xenolith	Mineral assemblage and hercynite morphology	Mineral analyzed	Zone	$\delta^{18}O$ (‰ VSMOW)
VB366	1534	Ryan's Pond	Massive	Anorthitic plagioclase	Hercynite	Core	5.1
VB366	1534	Ryan's Pond		Granular hercynite	Plagioclase	Core	5.6
VB366	1534	Ryan's Pond			Plagioclase	Matrix	7.0
VB433C	1266.4	Reid Brook	Dark-cored		Hercynite	Core	6.9
VB433C	1266.4	Reid Brook			Plagioclase	Overgrowth rim	9.1
VB462	631.7	North Eastern Deeps	Massive	Acciclar, granular hercynite	Hercynite	Core	5.9
VB462	631.7	North Eastern Deeps		Magnetite, anorthitic plagioclase	Hercynite	Core	6.2
VB479	483	Reid Brook	Dark-cored	Acciclar hercynite	Hercynite	Core	6.5
VB479	483	Reid Brook		Granular hercynite	Hercynite	Core	6.7
VB479	483	Reid Brook		Bulbous hercynite	Plagioclase	Core	7.0
VB479	483	Reid Brook		Magnetite	Plagioclase	Overgrowth rim	8.6
VB479	483	Reid Brook		Anorthitic plagioclase	Biotite	Overgrowth rim	5.6
VB479	483	Reid Brook			Plagioclase	Matrix	7.8
VB487	641	Reid Brook	Light-cored	Corundum	Plagioclase	Core	10.5
VB487	641	Reid Brook		Acciclar hercynite	Corundum	Core	5.9
VB487	641	Reid Brook		Magnetite	Hercynite	Rim	7.4
VB487	641	Reid Brook		Bulbous hercynite	Hercynite	Rim	7.6
VB487	641	Reid Brook		Granular hercynite	Plagioclase	Overgrowth rim	7.7
VB487	641	Reid Brook		Anorthitic plagioclase	Biotite	Overgrowth rim	5.6
VB487	641	Reid Brook			Plagioclase	Matrix	6.2
VB487	647	Reid Brook	Dark-cored	Anorthitic plagioclase	Hercynite	Core	10.3
VB487	647	Reid Brook		Granular hercynite	Plagioclase	Overgrowth rim	6.4
VB487	647	Reid Brook		Bulbous hercynite	Plagioclase	Matrix	9.0
VB487	656.1	Reid Brook	Variegated	Corundum	Corundum	Core	5.8
VB487	656.1	Reid Brook		Acciclar hercynite	Plagioclase	Core	8.1
VB487	656.1	Reid Brook		Anorthitic plagioclase	Hercynite	Core	7.8
VB487	656.1	Reid Brook		Bulbous hercynite	Hercynite	Core	7.8
VB487	656.1	Reid Brook		Granular hercynite	Plagioclase	Core	9.4
VB487	656.1	Reid Brook			Plagioclase	Overgrowth rim	8.4
VB487	656.1	Reid Brook			Plagioclase	Matrix	6.5
VB487	719.8	Reid Brook	Massive	Magnetite	Hercynite	Core	6.6
VB487	719.8	Reid Brook		Bulbous, acciclar hercynite	Hercynite	Core	6.2
VB487	719.8	Reid Brook		Anorthitic plagioclase	Plagioclase	Core	7.6
VB487	719.8	Reid Brook		Granular hercynite	Plagioclase	Matrix	8.1
VB488	435.6	North Eastern Deeps	Light-cored	Corundum, magnetite	Corundum	Core	6.4
VB488	435.6	North Eastern Deeps		Granular, acicular hercynite	Plagioclase	Core	10.4
VB488	435.6	North Eastern Deeps		Anorthitic plagioclase	Hercynite	Core	6.1
VB488	435.6	North Eastern Deeps			Plagioclase	Overgrowth rim	6.6
VB488	435.6	North Eastern Deeps			Plagioclase	Matrix	6.3
VB488	517.5	North Eastern Deeps	Light-cored	Corundum, accicular hercynite	Plagioclase	Core	10.7
VB488	517.5	North Eastern Deeps		Anorthitic plagioclase	Plagioclase	Core	10.9
VB488	517.5	North Eastern Deeps		Granular hercynite	Corundum	Core	4.1
VB488	517.5	North Eastern Deeps			Hercynite	Rim	7.3
VB488	517.5	North Eastern Deeps			Biotite	Overgrowth rim	5.5
VB488	517.5	North Eastern Deeps			Plagioclase	Matrix	7.0
VB488	517.5	North Eastern Deeps			Plagioclase	Matrix	7.0
VB492	974.6	S. Eastern Deeps	Dark-cored	Hercynite	Hercynite	Core	6.7
VB492	974.6	S. Eastern Deeps		Plagioclase	Plagioclase	Overgrowth rim	6.2
VB492	974.6	S. Eastern Deeps			Biotite	Overgrowth rim	5.3
VB492	974.6	S. Eastern Deeps			Plagioclase	Matrix	6.7
VB492	1005	S. Eastern Deeps		Plagioclase	Corundum	Core	4.1
VB492	1005	S. Eastern Deeps	Light-cored	Corundum	Corundum	Core	3.9
VB492	1005	S. Eastern Deeps			Plagioclase	Core	7.1
VB492	1005	S. Eastern Deeps			Biotite	Overgrowth rim	5.1
VB492	1032.2	S. Eastern Deeps	Dark-cored		Biotite	Overgrowth rim	5.5
VB501	707	Discovery Hill	Dark-cored		Biotite	Overgrowth rim	5.5

(*continued on next page*)

Table 2 (*continued*)

Core No.	Depth	Environment	Type of xenolith	Mineral assemblage and hercynite morphology	Mineral analyzed	Zone	$\delta^{18}O$ (‰ VSMOW)
VB501	711.8	Discovery Hill	Dark-cored		Viotite	Overgrowth rim	5.3
VB501	712.5	Discovery Hill	Light-cored	Corundum	Plagioclase	Core	8.3
VB501	712.5	Discovery Hill		Acciclar hercynite	Plagioclase	Core	8.2
VB501	712.5	Discovery Hill		Granular hercynite	Plagioclase	Core	9.3
VB501	712.5	Discovery Hill		Anorthitic plagioclase	Plagioclase	Core	7.8
VB501	712.5	Discovery Hill		Magnetite	Corundum	Core	6.6
VB501	712.5	Discovery Hill			Corundum	Core	7.5
VB501	712.5	Discovery Hill			Corundum	Core	6.1
VB501	712.5	Discovery Hill			Hercynite	Rim	7.6
VB501	712.5	Discovery Hill			Hercynite	Rim	5.1
VB501	712.5	Discovery Hill			Hercynite	Rim	6.2
VB501	712.5	Discovery Hill			Plagioclase	Overgrowth rim	8.5
VB501	712.5	Discovery Hill			Biotite	Overgrowth rim	5.4
VB501	712.5	Discovery Hill			Plagioclase	Matrix	7.4
VB510	566.2	Eastern Deeps	Dark-cored	Magnetite	Hercynite	Core	6.3
VB510	566.2	Eastern Deeps		Acciclar hercynite	Hercyniye	Core	6.2
VB510	566.2	Eastern Deeps		Anorthitic plagioclase	Plagioclase	Overgrowth rim	6.8
VB510	566.2	Eastern Deeps			Biotite	Overgrowth rim	5.4
VB510	566.2	Eastern Deeps			Biotite	Overgrowth rim	5.4
VB510	566.2	Eastern Deeps			Plagioclase	Matrix	6.5
VB510	607	Eastern Deeps	Massive	Acciclar hercynite	Hercynite	Core	6.4
VB510	607	Eastern Deeps		Vemicular hercynite	Hercynite	Core	6.1
VB510	607	Eastern Deeps		Magnetite	Hercynite	Core	5.7
VB510	607	Eastern Deeps		Granular hercynite	Hercynite	Core	5.9
VB510	607	Eastern Deeps		Anorthitic plagioclase	Plagioclase	Matrix	6.1
VB510	629	Eastern Deeps	Dark-cored	Anorthitic Plagioclase	Plagioclase	Overgrowth rim	8.0
VB510	629	Eastern Deeps		Hercynite	Plagioclase	Overgrowth rim	7.9
VB522	501	Discovery Hill	Light-cored	Acicular hercynite	Corundum	Core	5.8
VB522	501	Discovery Hill		Granular hercynite	Corundum	Core	5.5
VB522	501	Discovery Hill		Anorthitic plagioclase	Corundum	Core	4.1
VB522	501	Discovery Hill		Corundum	Plagioclase	Core	8.5
VB522	501	Discovery Hill			Plagioclase	Core	9.9
VB522	501	Discovery Hill			Plagioclase	Core	9.6
VB522	501	Discovery Hill			Hercynite	Rim	5.7
VB522	501	Discovery Hill			Biotite	Overgrowth rim	6.0
VB522	501	Discovery Hill			Biotite	Overgrowth rim	5.1
VB522	501	Discovery Hill			Plagioclase	Matrix	9.4
VB522	582	Discovery Hill			Biotite	Overgrowth rim	6.0
VB523	762	Eastern Deeps	Light-cored	Bulbous hercynite	Plagioclase	Core	6.2
VB523	762	Eastern Deeps		Corundum, magnetite	Hercynite	Rim	5.6
VB523	762	Eastern Deeps		Anorthitic plagioclase	Plagioclase	Overgrowth rim	7.5
VB523	762	Eastern Deeps		Granular hercynite	Biotite	Overgrowth rim	6.2
VB523	762	Eastern Deeps			Plagioclase	Matrix	6.1
VB531	877.5	Eastern Deeps	Light-cored	Magnetite	Plagioclase	Core	10.3
VB531	877.5	Eastern Deeps		Acciclar hercynite	Plagioclase	Core	10.7
VB531	877.5	Eastern Deeps		Granular hercynite	Corundum	Core	5.2
VB531	877.5	Eastern Deeps		Anorthitic plagioclase	Corundum	Core	5.7
VB531	877.5	Eastern Deeps		Corundum	Corundum	Core	3.8
VB531	877.5	Eastern Deeps			Hercynite	Rim	5.7
VB531	877.5	Eastern Deeps			Plagioclase	Overgrowth rim	7.1
VB531	877.5	Eastern Deeps			Plagioclase	Overgrowth rim	7.2
VB531	877.5	Eastern Deeps			Biotite	Overgrowth rim	5.4
VB531	877.5	Eastern Deeps			Plagioclase	Matrix	6.4
VB531	915.6	Eastern Deeps	Banded	Acciclar hercynite	Hercynite	Core	6.1
VB531	915.6	Eastern Deeps		Granular hercynite	Hercynite	Core	8.7
VB531	915.6	Eastern Deeps		Anorthitic plagioclase	Hercynite	Core	6.8
VB531	915.6	Eastern Deeps		Magnetite	Plagioclase	Overgrowth rim	7.7
VB531	915.6	Eastern Deeps			Biotite	Overgrowth rim	6.8

Table 2 (*continued*)

Core No.	Depth	Environment	Type of xenolith	Mineral assemblage and hercynite morphology	Mineral analyzed	Zone	$\delta^{18}O$ (‰ VSMOW)
VB531	915.6	Eastern Deeps			Plagioclase	Matrix	6.6
VB531	931	Eastern Deeps	Light-cored	Granular hercynite	Plagioclase	Core	7.3
VB531	931	Eastern Deeps		Anorthitic plagioclase	Corundum	Core	4.5
VB531	931	Eastern Deeps		Acciclar hercynite	Hercynite	Rim	6.1
VB531	931	Eastern Deeps		Corundum	Hercynite + plg	Rim	6.2
VB531	931	Eastern Deeps		Magnetite	Plagioclase	Core	6.4
VB531	931	Eastern Deeps			Plagioclase	Overgrowth rim	7.0
VB531	931	Eastern Deeps			Biotite	Overgrowth rim	5.4
VB531	931	Eastern Deeps			Plagioclase	Matrix	6.6
VB534A	1090.5	Red Dog	Light-cored	Granular hercynite	Plagioclase	Core	7.7
VB534A	1090.5	Red Dog		Corundum	Plagioclase	Core	7.2
VB534A	1090.5	Red Dog		Acciclar hercynite	Plagioclase	Core	8.4
VB534A	1090.5	Red Dog		Anorthitic plagioclase	Corundum	Core	4.5
VB534A	1090.5	Red Dog		Magnetite	Corundum	Core	2.4
VB534A	1090.5	Red Dog			Corundum	Core	2.0
VB534A	1090.5	Red Dog			Hercynite	Rim	5.2
VB534A	1090.5	Red Dog			Hercynite	Rim	5.4
VB534A	1090.5	Red Dog			Plagioclase	Overgrowth rim	6.9
VB534A	1090.5	Red Dog			Plagioclase	Overgrowth rim	6.7
VB534A	1090.5	Red Dog			Plagioclase	Matrix	5.7
VB534A	1090.5	Red Dog			Plagioclase	Matrix	7.5
VB534A	1094.5	Red Dog	Dark-cored	Acciclar hercynite	Hercynite	Core	5.8
VB534A	1094.5	Red Dog		Anorthitic plagioclase	Plagioclase	Core	6.7
VB534A	1094.5	Red Dog		Magnetite	plagioclase	Overgrowth rim	6.1
VB534A	1094.5	Red Dog		Granular hercynite	Biotite	Overgrowth rim	5.0
VB535	1004	Far Eastern Deeps	Light-cored	Corundum	Plagioclase	Core	7.1
VB535	1004	Far Eastern Deeps		Acciclar hercynite	Plagioclase	Core	7.5
VB535	1004	Far Eastern Deeps		Granular hercynite	Corundum	Core	5.4
VB535	1004	Far Eastern Deeps		Anorthitic plagioclase	Corundum	Core	3.9
VB535	1004	Far Eastern Deeps		Magnetite	corundum	Core	5.7
VB535	1004	Far Eastern Deeps			Hercynite	Rim	5.2
VB535	1004	Far Eastern Deeps			Hercynite	Rim	6.9
VB535	1004	Far Eastern Deeps			Plagioclase	Overgrowth rim	7.2
VB535	1004	Far Eastern Deeps			Plagioclase	Overgrowth rim	6.2
VB535	1004	Far Eastern Deeps			Biotite	Overgrowth rim	5.1
VB535	1004	Far Eastern Deeps			Plagioclase	Matrix	6.1
VB535	1008.2	Far Eastern Deeps	Dark-cored		Biotite	Overgrowth rim	6.0
VB535	1016.8	Far Eastern Deeps	Light-cored	Magnetite	Plagioclase	Core	10.6
VB535	1016.8	Far Eastern Deeps		Corundum	Corundum	core	5.2
VB535	1016.8	Far Eastern Deeps		Acciclar hercynite	Hercynite	Core	6.3
VB535	1016.8	Far Eastern Deeps		Granular hercynite	Plagioclase	overgrowth rim	10.7
VB535	1016.8	Far Eastern Deeps			Plagioclase	Matrix	6.7
VB535	1016.8	Far Eastern Deeps			Plagioclase	Matrix	5.9
VB549	783.9	Far Eastern Deeps	Light-cored	Corundum	Plagioclase	Core	9.3
VB549	783.9	Far Eastern Deeps		Acciclar hercynite	Corundum	Core	6.3
VB549	783.9	Far Eastern Deeps		Anorthitic plagioclase	Hercynite	Rim	8.5
VB549	783.9	Far Eastern Deeps		Magnetite	Hercynite	Rim	6.5
VB549	783.9	Far Eastern Deeps			Plagioclase	Overgrowth rim	7.1
VB549	783.9	Far Eastern Deeps			Plagioclase	Overgrowth rim	10.5
VB549	783.9	Far Eastern Deeps			Biotite	Overgrowth rim	6.2
VB549	983.9	Far Eastern Deeps	Dark-cored	Acicular hercynite	Hercynite	Core	6.4
VB549	983.9	Far Eastern Deeps		Anorthitic plagioclase	Plagioclase	Overgrowth rim	8.6
VB549	983.9	Far Eastern Deeps		Granular hercynite	Plagioclase	Matrix	7.1
VB549	989.7	Far Eastern Deeps	Massive		Hercynite	Core	7.3
VB555	1639.8	Ryan's Pond	Dark-cored	Magnetite	Hercynite	Core	2.9
VB555	1639.8	Ryan's Pond		Hercynite	Plagioclase	Overgrowth rim	8.3
VB555	1639.8	Ryan's Pond	Variegated	Plagioclase	Plagioclase	Matrix	8.2
VB555	1668	Ryan's Pond	Dark-cored	Granular hercynite	Hercynite	Core	7.4

(*continued on next page*)

Table 2 (*continued*)

Core No.	Depth	Environment	Type of xenolith	Mineral assemblage and hercynite morphology	Mineral analyzed	Zone	$\delta^{18}O$ (‰ VSMOW)
VB555	1668	Ryan's Pond			Plagioclase	Overgrowth rim	9.0
VB555	1668	Ryan's Pond			Plagioclase	Matrix	5.6

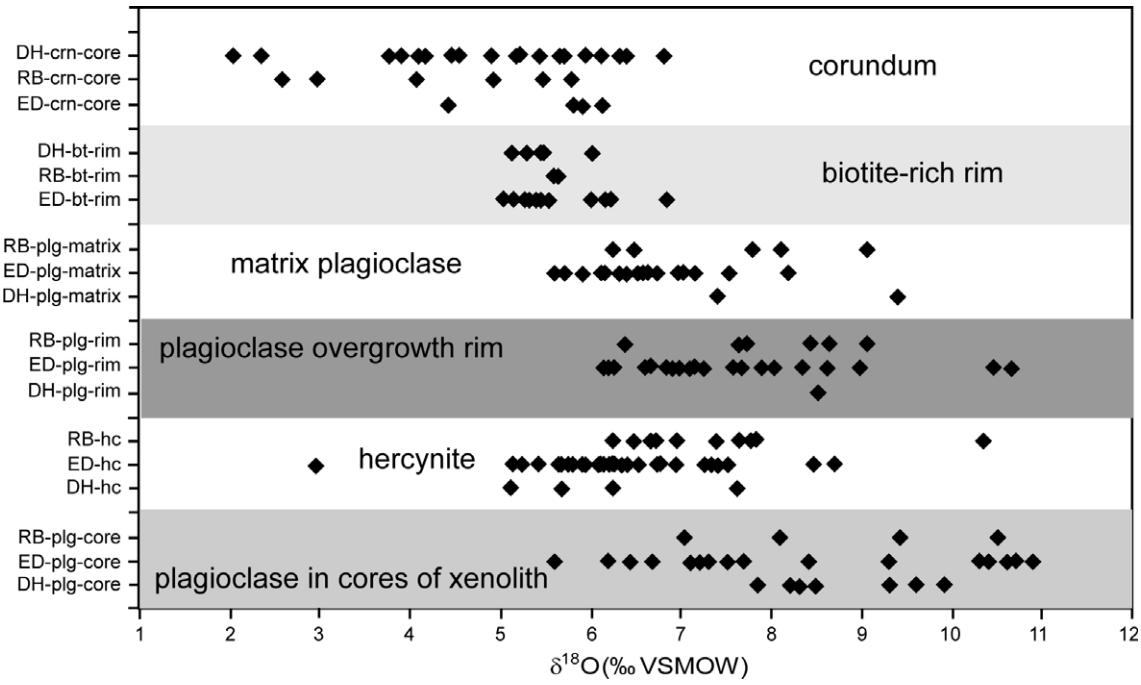

Fig. 7. Ranges of $\delta^{18}O$ values of biotite (bt), plagioclase (plg), hercynite (hc), and corundum (crn) separates from cores, rims and enclosing igneous matrix of xenoliths from the Eastern Deeps (ED, including Ryan's Pond and Red Dog), Discovery Hill (DH), and Reid Brook (RB) zones of the Voisey's Bay Intrusion.

Table 3
$\delta^{18}O$ and δD values of biotite bands that surround xenoliths

Sample No.	Depth	Section	$\delta^{18}O$(‰ VSMOW)	δD (‰ VSMOW)
VB501	711.8	Discovery Hill	5.3	−80
VB501	707	Discovery Hill	5.5	−77
VB522	582	Discovery Hill	6.0	−62
VB510	566.2	Eastern Deeps	5.4	−72
VB523	762	Eastern Deeps	6.2	−60
VB531	877.5	Eastern Deeps	5.4	−73
VB535	1008.2	Far Eastern Deeps	6.0	−58
VB549	783.9	Far Eastern Deeps	6.2	−60
VB488	517.5	North Eastern Deeps	5.5	−60
VB534A	1094.5	Red Dog	5.0	−78
VB479	483	Reid Brook	5.6	−79
VB487	656.1	Reid Brook	5.5	−78
VB487	641	Reid Brook	5.6	−76
VB492	1005	S. Eastern Deeps	5.1	−79
VB492	1032.2	S. Eastern Deeps	5.5	−78

that consist of biotite, garnet, pyroxene, plagioclase, and cordierite (5.2–10.8‰). Such variations of $\delta^{18}O$ values in the Tasiuyak Gneiss are important in the assessment of the $\delta^{18}O$ values of the contaminated magma.The high bulk $\delta^{18}O$ values of the Tasiuyak Gneiss suggest that $\delta^{18}O$ measurements of igneous rocks should be sensitive indicators of magma contamination by the Tasiuyak Gneiss. The range of $\delta^{18}O$ values obtained for the enderbitic and the Archean mafic gneisses (5.2–7.9‰) is generally consistent with their intermediate to mafic igneous rock parentage. Oxygen isotopes are thus not useful indicators of potential contamination of mafic magma by these country rocks.

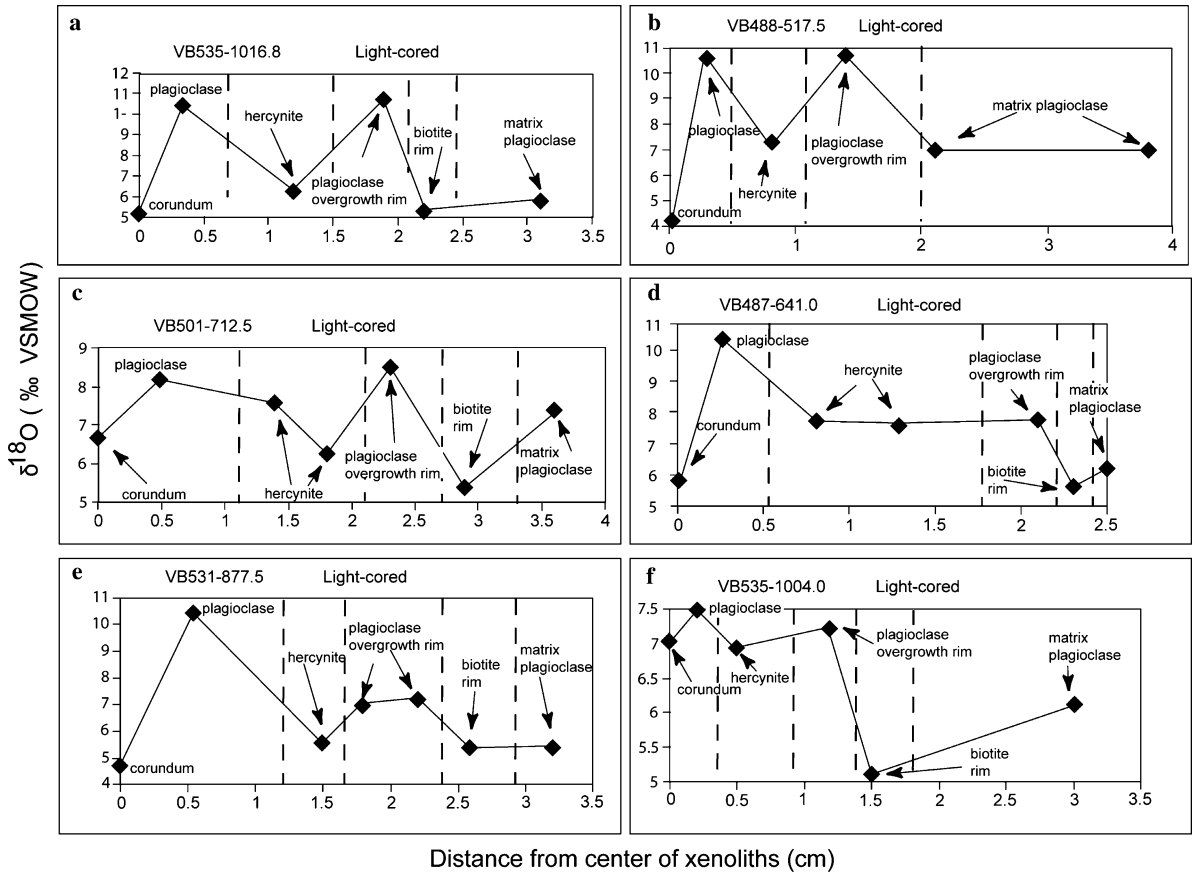

Fig. 8. Examples of $\delta^{18}O$ profiles of xenoliths from the Voisey's Bay Intrusion. Because corundum separates were collected from entire cores of light-cored xenoliths the delta value is plotted at the origin of the profile.

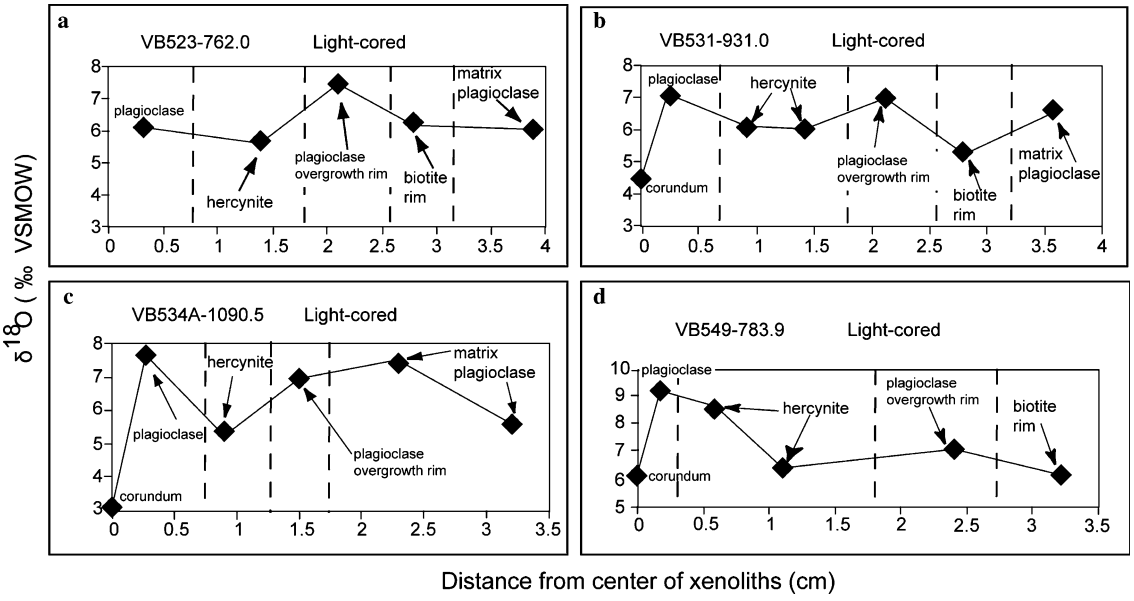

Fig. 9. Examples of $\delta^{18}O$ profiles of xenoliths from the Voisey's Bay Intrusion.

The high $\delta^{18}O$ values for quartz and feldspar from the Archean quartzofeldspathic gneiss suggest that assimilation of these rocks by mafic magma could cause significant perturbations to normal mantle $\delta^{18}O$ signatures. Considerable overlap in the ranges of $\delta^{18}O$ values of the Tasiuyak Gneiss and the Archean quartzofeldspathic gneiss makes it difficult to distinguish their relative roles as magma contaminants based on oxygen isotopic values alone. Bulk

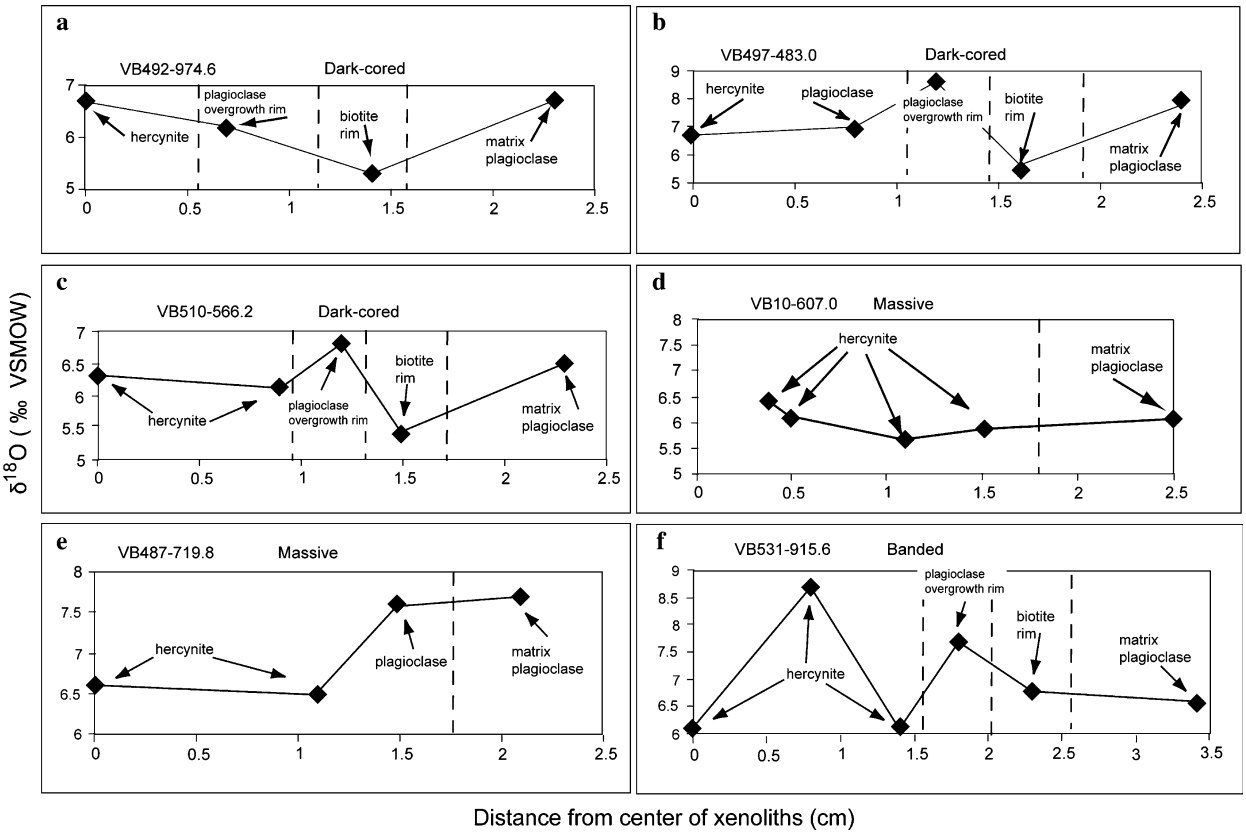

Fig. 10. Examples of $\delta^{18}O$ profiles of xenoliths from the Voisey's Bay Intrusion.

assimilation of high-^{18}O contaminants has been suggested for many intrusions that are characterized by anomalously high $\delta^{18}O$ values (e.g., Sparks, 1986; Schiffries and Rye, 1989; Halama et al., 2004; Harris et al., 2004). However, because bulk assimilation did not occur in the Voisey's Bay Intrusion as evidenced by the presence of refractory minerals in the xenoliths, contamination must be evaluated in terms of incongruent dissolution, or partial melting. Several studies have demonstrated that incongruent dissolution and partial melting processes can alter the geochemical signatures of magmatic rocks during assimilation (e.g., Taylor, 1980; DePaolo, 1981; Lesher and Burnham, 1999; Spera and Bohrson, 2001).

The $\Delta^{18}O$ values of mineral pairs from the Tasiuyak, enderbitic, and Archean gneisses are shown in Table 4. Calculated oxygen isotopic equilibration temperatures for mineral pairs from the Tasiuyak Gneiss range between 560 and >1100 °C. The range of calculated temperatures for the Archean quartzofeldspathic gneiss is relatively low (505–530 °C) compared to those obtained from the

Table 4
Oxygen isotope thermometry using regional and contact aureole mineral pairs

Sample No.	Rock type	Assemblage	$\Delta_{qtz\text{-}gnt}$	$\Delta_{plg\text{-}gnt}$	$\Delta_{qtz\text{-}plg}$	$\Delta_{qtz\text{-}px}$	$\Delta_{qtz\text{-}bt}$	$\Delta_{qtz\text{-}K\text{-}feld}$
VB192-293	T.G.	Aureole	3.6 (655)	2.4 (595)	1.2 (770)	3.3 (640)	5.2 (525)	
TG-1	T.G.	Regional	3.5 (670)	2.0 (675)	1.5 (660)	3.9 (565)		
TG-2	T.G.	Regional	3.5 (670)	2.4 (595)	1.1 (815)	3.6 (600)		
TG3	T.G.	Regional	3.4 (680)	2.3 (610)	1.1 (815)	3.6 (600)		
VB433-107	T.G.	Regional		2.6 (560)				
VB433-109	T.G.	Regional			1.2 (770)	3.7 (590)		
VB433-115	T.G.	Regional		2.5 (575)	0.6 (>1100)	3.0 (685)		
AG-1	A.G.	Regional					5.3 (520)	1.5 (530)
AG-2	A.G.	Regional					5.5 (505)	
AG-3	A.G.	Regional					5.4 (510)	
AG-4	A.G.	Regional					5.1 (530)	

T.G., Tasiuyak Gneiss; A.G., Archean gneiss; gnt, garnet; qtz, quartz; bt, biotite; plg, plagioclase; K-feld, K-feldspar; px, pyroxene; (660), temperature (°C) corresponding to the Δ value. Temperatures using qtz-gnt from Sharp (1995), qtz-plg from Clayton et al. (1989), qtz-px from Chiba et al. (1989), qtz-gnt from Bottinga and Javoy (1975), and qtz-K-Feld from Zheng (1993).
Uncertainities calculated using ±0.1‰ vary from 15 to 50 °C.

Tasiuyak Gneiss. A Δ value of 1.6 ± 0.1 for a quartz and alkali feldspar pair from the quatzofeldspathic gneiss is consistent with cooling and diffusive exchange in a closed system (e.g., Jenkin et al., 1991; Eiler et al., 1993). Low temperatures obtained from mineral pairs using biotite may be indicative of the low closing temperature of biotite or isotopic exchange during retrogression and low-temperature alteration. The majority of quartz-plagioclase mineral pairs indicate temperatures between 660 and 815 °C, which is consistent with the results of previous studies based on mineral equilibria (e.g., Berg and Docka, 1983; Lee, 1987; McFarlane et al., 2003). However, the wide range of temperatures recorded by the entire system indicate oxygen isotopic disequilibrium, which is consistent with expected isotopic trends in rocks that contain both high (garnet, pyroxene, quartz) and low (biotite, plagioclase, K-feldspar) closing temperature minerals (e.g., Eiler et al., 1993).

6.2. Prediction of $\delta^{18}O$ variations in minerals from the Tasiuyak Gneiss during closed-system contact metamorphism

Modeling of $\delta^{18}O$ variations in the contact aureole of the Voisey's By Intrusion provides a basis for the further evaluation of $\delta^{18}O$ fractionation that accompanies magma–xenolith interaction. We use the Tasiuyak Gneiss as a starting composition to model the progressive transformation of pelitic protolith mineral assemblages and associated oxygen isotopic exchange. Typical Tasiuyak Gneiss consists of garnet, sillimanite, feldspars, pyroxene, quartz, and biotite. The presence of garnet atolls and vermicular symplectites of cordierite plus orthopyroxene plus K-feldspar in the Tasiuyak Gneiss hornfels indicates that the reactions during contact metamorphism were characterized by the breakdown of garnet, biotite, and possibly sillimanite. The breakdown of biotite and garnet in the hornfels may be represented by the following net-transfer reaction:

$$\underset{\text{Biotite}}{2KFe_3AlSi_3O_{10}(OH)_2} + \underset{\text{Garnet}}{2Fe_3Al_2Si_3O_{12}} + \underset{\text{Quartz}}{9SiO_2} = \underset{\text{Cordierite}}{Fe_2Al_4Si_5O_{18}(H_2O)_2} + \underset{\text{Orthopyroxene}}{10FeSiO_3} + \underset{\text{K-feldspar}}{2KAlSi_3O_8}\,. \quad (1)$$

We have modeled closed-system isothermal and polythermal oxygen isotopic exchange for reaction (1) using mass balance procedures similar to those described by Rumble and Spear (1983) and Chamberlain et al. (1990), and isotopic fractionation factors from Bottinga and Javoy (1975), Zheng (1991, 1993), Sharp (1995), and Zhao and Zheng (2003).

Three calculations of isothermal exchange at 800 °C were done using various proportions of biotite, quartz and garnet to evaluate the effect of modal abundances on the $\delta^{18}O$ values of both reactant and product minerals of the reaction. Initial $\delta^{18}O$ values for garnet (35%), biotite (46%), and quartz (19%) were 8.9‰, 9.2‰, and 12.7‰, respectively, with a bulk $\delta^{18}O$ value of 10.0‰. Iterative (100 step) calculations produce $\delta^{18}O$ values of cordierite, K-feldspar, and orthopyroxene of 10.2‰, 11.4‰, and 9.1‰, respectively. Varying the modal percentages of garnet (35–29%), biotite (46–39%), and quartz (19–32%) produced resultant variations in the $\delta^{18}O$ values of garnet, biotite, quartz, cordierite, orthopyroxene, and K-feldspar of less than 0.7‰.

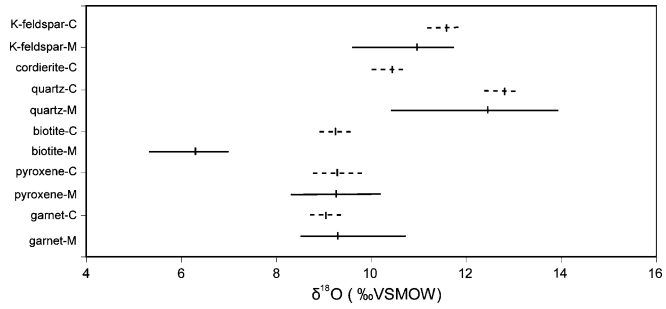

Fig. 11. A comparison of calculated and measured $\delta^{18}O$ values of garnet, biotite, pyroxene, cordierite, K-feldspar, and quartz from the Tasiuyak Gneiss in the contact aureole of the Voisey's Bay Intrusion. M, measured and C, calculated. Broken lines represent calculated values and continuous lines represent measured values. Tic marks along the lines correspond to average values.

Polythermal calculations of oxygen isotope exchange from 800 to 950 °C using the same initial modal percentages as above yield $\delta^{18}O$ values for cordierite, orthopyroxene, and K-feldspar that vary from 10.2‰ to 10.3‰, 9.0‰ to 9.8‰, and 11.4‰ to 11.6‰, respectively. The $\delta^{18}O$ values of the reactants garnet, biotite, and quartz vary by less than 0.4‰ relative to their initial values.

Fig. 11 compares the measured and calculated (from isothermal and polythermal modelling) $\delta^{18}O$ values of minerals in the Tasiuyak Gneiss hornfels. The ranges of the modeled $\delta^{18}O$ values in the hornfels show considerable overlap with the measured values. The results are consistent with the premise that closed-system oxygen isotope exchange occurred during contact metamorphism. Ripley et al. (2002) discussed the fact that extensive prograde devolatilization reactions occurred more than 500 Ma before the emplacement of the Voisey's Bay Intrusion; the predominance of closed-system oxygen isotopic exchange in the contact aureole is consistent with this observation. Small changes in $\delta^{18}O$ values of the minerals indicate that chemical transfer during contact metamorphism was not important, except for possible dehydration of biotite. The low $\delta^{18}O$ values of biotite may indicate that an ^{18}O-rich volatile phase was lost from biotite as a result of dehydration melting.

6.3. Controls of $\delta^{18}O$ variations in xenoliths

Oxygen isotope variations in the different types of xenoliths in the Voisey's Bay Intrusion can be attributed to: (1) different protoliths; (2) variable extents of exchange with magma (residence time); (3) partial melting and infiltration of magmatic components into the xenoliths; and (4) subsolidus reequilibration and post-magmatic hydrothermal alteration.

The samples studied show no textural and mineralogical evidence for late stage interaction with fluids. Therefore, if ^{18}O-exchange occurred as a result of late stage fluid involvement, the process occurred in the absence of observable mineralogical alteration. Ripley et al. (2000) found no evidence for widespread perturbations to magmatic oxygen isotope signatures in the Voisey's Bay Intrusion, and hence we do not consider it likely that oxygen isotope variations in the xenoliths have been affected by low temperature fluids.

It is possible that some of the variations in $\delta^{18}O$ values of xenoliths are related to different protoliths. The determination of the exact source of the xenoliths is difficult because all xenoliths have similar mineral assemblages. Xenoliths with low bulk $\delta^{18}O$ values (<8‰) can be interpreted to have originated from any of the immediate country rocks. However, the light-cored xenoliths with $\delta^{18}O$ values that are higher than those obtained from the Archean mafic gneiss and the enderbitic gneiss could only have been derived from either the Tasiuyak Gneiss or the Archean quartzofeldspathic gneiss (see Figs. 6 and 7). The relatively high $\delta^{18}O$ values of plagioclase in the xenoliths from the Reid Brook, Eastern Deeps, and Discovery Hill zones (Fig. 7) also suggest that the xenoliths could have originated from either the Tasiuyak or the quartzofeldspathic gneisses. The preservation in some xenoliths of pseudomorphic textures of hercynite after key minerals found in the Tasiuyak Gneiss strongly suggests that the xenoliths were derived from the Tasiuyak Gneiss.

Prior to or upon incorporation into magma, a Tasiuyak Gneiss xenolith would start to transform into a hornfels via reactions such as (1). Subsequent interaction with the magma involving a series of reactions would transform the hornfels mineral assemblage into a refractory mineral assemblage and partial melt. We propose the following reactions to account for the formation of corundum, Ca-rich plagioclase and hercynite in the xenoliths

$$\underset{\text{Na-rich plagioclase}}{2.67(Na_{0.7}Ca_{0.3}Al_{1.3}Si_{2.7}O_8)_{(s)}} \Rightarrow \underset{\text{Corundum}}{0.835Al_2O_{3(s)}} + \underset{\text{Ca-rich Plagioclase}}{(Na_{0.2}Ca_{0.8}Al_{1.8}Si_{2.2}O_8)_{(s)}} + \underset{\text{Melt}}{0.835Na_2O_{(m)}} + 5SiO_{2(m)} \quad (2)$$

$$\underset{\text{K-feldspar}}{2KAlSi_3O_{8(s)}} \Rightarrow \underset{\text{Corundum}}{Al_2O_{3(s)}} + \underset{\text{Melt}}{K_2O_{(m)}} + 6SiO_{2(m)} \quad (3)$$

$$\underset{\text{Sillimanite}}{Al_2SiO_{5(s)}} \Rightarrow \underset{\text{Corundum}}{Al_2O_{3(s)}} + \underset{\text{Melt}}{SiO_{2(m)}} \quad (4)$$

$$\underset{\text{Garnet}}{Fe_3Al_2Si_3O_{12(s)}} \Rightarrow \underset{\text{Hercynite}}{FeAl_2O_{4(s)}} + \underset{\text{Melt}}{3SiO_{2(m)}} + 2FeO_{(m)} \quad (5)$$

$$\underset{\text{Pyroxene}}{FeSiO_{3(s)}} + \underset{\text{Sillimanite}}{Al_2SiO_{5(s)}} \Rightarrow \underset{\text{Hercynite}}{FeAl_2O_{4(s)}} + \underset{\text{Melt}}{2SiO_{2(m)}} \quad (6)$$

$$\underset{\text{Cordierite}}{Fe_2Al_4Si_5O_{18(s)}} \Rightarrow \underset{\text{Hercynite}}{2FeAl_2O_{4(s)}} + \underset{\text{Melt}}{5SiO_{2(m)}} \quad (7)$$

$$\underset{\text{Corundum}}{Al_2O_{3(s)}} + \underset{\text{Magma/melt}}{FeO_{(m)}} \Rightarrow \underset{\text{Hercynite}}{FeAl_2O_{4(s)}} \quad (8)$$

For simplicity, only Fe end-members of the Fe–Mg solid solutions are used in the reactions (2-8). A xenolith from a typical leucosome of the Tasiuyak Gneiss would react with the magma to yield an initial restite assemblage of corundum and Ca-rich plagioclase via reactions such as 2, 3, and 4. Depending on the quartz/feldspar ratio in the leucosomal xenolith, partial melts of various Si contents could have been generated during the formation of the refractory corundum-plagioclase assemblage. Continual reaction with magma would have lead to metasomatic infiltration of FeO and MgO, resulting in conversion of corundum to hercynite via reaction (8). Mariga et al. (2006) have shown that the Fe–Mg depletion in the plagioclase-rich overgrowth rim surrounding the xenoliths balances the Fe–Mg enrichment in the hercynite zone within the xenoliths (Fig. 5). A xenolith from melanosomes of the Tasiuyak Gneiss would react with the magma to form hercynite, magnetite, and Ca-rich plagioclase via reactions such as 5, 6, and 7. The amount of Ca-rich plagioclase in this type of xenolith depends on the original proportion of plagioclase in the xenolith. Because xenoliths from the melanosomes of the Tasiuyak Gneiss contain a significant proportion of ferromagnesian minerals (biotite, garnet, pyroxene, and cordierite), diffusion of Fe and Mg from the enclosing magma to xenoliths was less important than for the xenoliths of the leucosomes.

The measured $\delta^{18}O$ values of plagioclase (6.2–10.9‰) and corundum (2.0–6.8‰) found in the cores of xenoliths indicate that ^{18}O has been lost from the xenoliths. The causes of the isotopic shifts in the xenoliths must be in part related to loss of a partial melt, but later isotopic exchange with fresh magma must also be considered. In order to evaluate the $\delta^{18}O$ values of corundum, plagioclase, and partial melt we have modeled open (Rayleigh) and closed (batch melt extraction) system oxygen isotopic exchange during reaction (2) using an initial feldspar $\delta^{18}O$ value of 10.7‰; the results are presented graphically in Fig. 12. The absence of corundum in the hornfels indicates that reactions such as (2) that produced corundum must have occurred after the xenoliths were enclosed in magma (i.e., at considerably higher temperatures than those experienced in the contact aureole). Our calculations were performed at 1100 °C using the fractionation factors of Zheng (1993, 1991) and Zhao and Zheng (2003). Because the partial melt produced during xenolith–magma interaction would have been siliceous in composition we have used mineral fractionation factors relative to rhyolitic melt calculated by Zhao and Zheng (2003).

The $\delta^{18}O$ values of Ca-rich plagioclase, corundum and partial melt increase from 10.2‰ to 10.9‰, 6.7‰ to 7.4‰, and 10.8‰ to 11.5‰, respectively, with the progress of reaction (2) in an open system (Fig. 12). In a closed system the $\delta^{18}O$ values of Ca-rich plagioclase, corundum, and melt vary from 10.2‰ to 10.8‰, 6.7‰ to 7.2‰, and 10.8‰ to 11.4‰, respectively. The majority of measured $\delta^{18}O$ values of plagioclase (6.2–10.9‰) and corundum (2.0–6.8‰) are well below those predicted by both models. We offer two possibilities for the relative ^{18}O depletion in the corundum/feldspar cores of xenoliths. One is that a Rayleigh

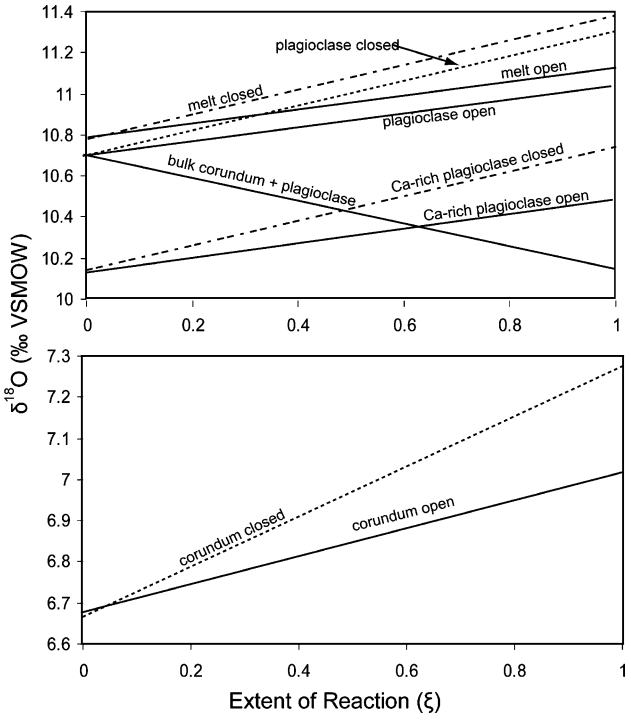

Fig. 12. Variations in oxygen isotope values produced during open and closed system conversion of Na–Ca-plagioclase to Ca-rich plagioclase, corundum and partial melt. The calculations were done at 1100 °C, following Reaction (2).

process of melt removal from the xenoliths occurred, but with a much larger melt-mineral fractionation than that which we employed. A larger Δ value of melt-mineral would be consistent with the computed $\delta^{18}O$ value of the expelled melt based on measured corundum and feldspar $\delta^{18}O$ values. A much more likely alternative is that the relatively low $\delta^{18}O$ values of corundum and plagioclase record an approach to isotopic equilibrium with surrounding ~5–6‰ mafic magma. In this scenario, an ^{18}O-rich melt similar to that predicted in the open system model would leave the xenolith, and in part mix with the enclosing magma. Synchronously with high-^{18}O melt expulsion, isotopic exchange between the residual corundum/feldspar assemblage and as yet uncontaminated mafic magma may have acted to lower corundum and plagioclase $\delta^{18}O$ values. Corundum that equilibrated with a 5–6‰ mafic magma would be expected to have a $\delta^{18}O$ value near 2.0–2.5‰. The lowest $\delta^{18}O$ values of corundum are in this range and lend credence to a model involving isotopic exchange with surrounding mafic magma. The variability in both corundum and plagioclase $\delta^{18}O$ values, as well as Δ (plagioclase-corundum) values which range from 0.3‰ to 6.5‰, suggest that isotopic equilibrium with the surrounding magma was not attained in the corundum bearing xenoliths, no matter which process of oxygen isotopic exchange and transport was dominant.

Part of the ^{18}O-rich partial melt that was lost from the xenoliths could have accumulated in the magma immediately surrounding the xenoliths where it crystallized to form the plagioclase and biotite rims (see Fig. 5). Moderate to slightly elevated $\delta^{18}O$ values of the plagioclase overgrowth surrounding some xenoliths are consistent with the premise that the magma immediately surrounding the xenoliths served as the sink for partial melt. It is essential to consider that the aluminous composition of the xenoliths requires that an extremely siliceous component was removed from the original assemblage. Mariga et al. (2006) have described a two-stage melting process where approximately 70% melting could have produced compositions that are similar to those of the light-cored xenoliths. This indicates that for a 3 cm diameter xenolith with a 0.5 cm band of plagioclase, the overgrowth band can account for only 45% of the oxygen lost from the initial xenolith. Two plagioclase rim samples have $\delta^{18}O$ values in excess of 10‰, suggesting that the bulk of their oxygen was derived from the ~11‰ melt lost from the xenolith (see Fig. 12). Most $\delta^{18}O$ values of the plagioclase bands are between 6‰ and 9‰ (Fig. 7), suggesting that either much smaller proportions of xenolith-derived melt was involved in mixing at the xenolith margin, or that isotopic exchange with uncontaminated mafic magma lowered the $\delta^{18}O$ value of the hybrid melt. The lack of any evidence for ^{18}O-enrichment throughout the igneous rocks of the Voisey's Bay Intrusion suggests that ^{18}O-rich oxygen from the xenoliths that cannot be accounted for by the plagioclase-rich band (in excess of 50% of the oxygen released from the xenoliths) was either mixed on a large scale or was removed by continuous flow of magma in a dynamic conduit system.

The $\delta^{18}O$ and δD values of the biotite band surrounding some xenoliths rims are not anomalous, and are similar to those of 'normal' magmatic biotite. Biotite crystallization is thought to be linked to K derived from the xenoliths accumulating in a boundary layer (see Fig. 5), and hence anomalous $\delta^{18}O$ values might be expected. However, although the $\delta^{18}O$ values of the plagioclase overgrowth may be greater than that of the enclosing magma, the oxygen and hydrogen isotopic values of biotite bands strongly suggest that biotite has equilibrated with uncontaminated mafic magma. The biotite band may have, in essence, buffered the plagioclase from more extensive exchange with surrounding magma.

6.4. Hercynite $\delta^{18}O$ values and extent of xenolith equilibration with mafic magma

Reactions 5 through 7 generate hercynite as a product of the breakdown of garnet, pyroxene, or cordierite. However, a large proportion of hercynite that is present in the xenoliths within the Voisey's Bay Intrusion formed as a result of replacement of corundum. The replacement front is particularly well defined in light-cored xenoliths with dark (hercynite-rich) rinds (Fig. 4). This relationship suggests that the transport of ^{18}O-rich partial melt out of the xenoliths may have been coupled with the inward transport of FeO and MgO, providing the potential for complex oxygen isotopic exchange (see Fig. 5). The $\delta^{18}O$ value of hercynite

that replaced corundum was controlled by the initial value of corundum (shown above to be variable) and the extent of equilibration with the enclosing magma. If the magma $\delta^{18}O$ value was near 5.5‰ the isotopic value of equilibrated hercynite would have been ~2.7‰ at 1100 °C. As is the case with corundum, measured $\delta^{18}O$ values of hercynite are generally higher than this value, and spatially variable. $\delta^{18}O$ values of hercynite that replaces acicular corundum range from 2.9‰ to 7.6‰, and strongly suggest that oxygen isotopic equilibrium with mafic magma was not attained.

7. Conclusions: oxygen isotopic variations in and around xenoliths in the Voisey's Bay Intrusion

The processes discussed above can be utilized to evaluate the oxygen isotope profiles of the xenoliths in the Voisey's Bay Intrusion. Upon incorporation into the magma leucosomal xenoliths that contain quartz and feldspar were likely to have had uniform (flat) $\delta^{18}O$ profiles. Heating to a temperature near that of the magma (~1100 °C) would lead to the generation of an ^{18}O-rich partial melt, as well as refractory corundum and Ca-rich plagioclase. Rapid loss of the partial melt to the magma may have in part been responsible for non-equilibrium corundum-plagioclase Δ values, as well as spatially variable $\delta^{18}O$ values. Part of the ^{18}O-enriched melt collected in a Si, Al, and Ca-rich boundary layer around the xenolith where it crystallized to form the plagioclase overgrowth rims. Potassium enrichment due to advective transport out of the xenolith, as well as exclusion from the zone of plagioclase crystallization, led to the crystallization of biotite, which insulated the plagioclase rim and xenolith from further exchange with magma. At least locally some of the high-^{18}O melt was lost to passing magma. Isotopic exchange between biotite and magma led to mantle-like $\delta^{18}O$ and δD values of the biotite rim.

Xenoliths with high proportions of corundum are generally characterized by relatively low $\delta^{18}O$ values in their cores (e.g., Fig. 9) In contrast, xenoliths with relatively low proportions of corundum and higher amounts of plagioclase have elevated $\delta^{18}O$ values in their cores (e.g., Fig. 8). These variations relate to both variable protolith mineralogy and extents of partial melting, and attest to the general non-equilibrium state of the system. Infiltration of FeO and MgO from magma into the xenoliths led to the replacement of corundum by hercynite. Hercynite $\delta^{18}O$ values are typically higher than those expected for equilibrium with mantle-derived mafic magma, in part related to exchange with high-^{18}O hybrid melt formed at the xenolith margin. Where plagioclase and biotite rims did not prevent interaction with enclosing magma, continued exchange and FeO–MgO infiltration has led to the formation of hercynite-rich, massive xenoliths.

Xenoliths from the melanosomes are also likely to have been characterized by flat (uniform) $\delta^{18}O$ profiles at the time of incorporation into the magma. Hercynite in these xenoliths may have been produced as a result of the breakdown of garnet, pyroxene, and cordierite, and hence may have inherited relatively high $\delta^{18}O$ values (e.g., Figs. 9d and 10f). Plagioclase is expected to have undergone a similar series of reactions to those outlined above. In the final assemblage hercynite would have been produced by thermal decomposition of ferromagnesian minerals as well as by the replacement of corundum. The variability in hercynite $\delta^{18}O$ values strongly suggests that oxygen isotopic equilibration with the enclosing magma was not attained.

The $\delta^{18}O$ values of minerals in xenoliths from the Voisey's Bay Intrusion record a geochemical history that includes rapid thermal equilibration with magma and the production of a refractory mineral assemblage. High ^{18}O partial melts were generated from quartz-and feldspar bearing protoliths (either metasedimentary or in the case of quartzofeldspathic gneisses, potentially high-^{18}O granitic rocks), and a portion of this melt was dispersed in magma that passed through the conduit system. As detailed by Li and Ripley (2005) the mixing of a siliceous partial melt with a basaltic magma could induce sulfide saturation, which is a necessary requirement for the generation of magmatic Cu–Ni–PGE ores. Continued reaction with magma led to the replacement of corundum in xenoliths by hercynite, but oxygen isotopic equilibration with basaltic magma was not attained. Detailed isotopic studies at a grain scale are required to better evaluate both magma-mineral reaction mechanisms and potential exchange during retrograde cooling.

Acknowledgments

This work was supported by National Science Foundation Grant Ear 0086538 to E.M.R. We acknowledge constructive criticisms and reviews by James Brophy, Robert Wintsch, Erika Elswick, Peter Larson, and Zach Sharp. Dave Cole provided excellent editorial supervision. Staff and geologists of the Voisey's Bay Nickel Company, particularly Dan Lee and Dawn Evans-Lamswood, are thanked for granting access to samples and for constructive discussions. Steve Studley, Jon Fong, Peter Sauer, and Arndt Schimmelmann of the Indiana University Stable Isotope Research Facility are thanked for technical assistance.

Associate editor: David R. Cole

References

Amelin, Y., Li, C., Naldrett, A.J., 1999. Geochronology of the Voisey's Bay intrusion, Labrador, Canada, by precise U–Pb dating of coexisting baddeleyite, zircon, and apatite. *Lithos* **47**, 33–51.

Amelin, Y., Li, C., Valayevo, O., Naldrett, A.J., 2000. Nd–Pb–Sr isotope systematics of crustal assimilation in the Voisey's Bay Mushuau Intrusions, Labrador, Canada. *Econ. Geol.* **95**, 815–830.

Berg, J., Docka, J., 1983. Geothermometry in the Kiglapait contact aureole, Labrador. *Am. J. Sci.* **283**, 414–434.

Bottinga, Y., Javoy, M., 1975. Oxygen isotope partitioning among the minerals in igneous and metamorphic rocks. *Rev. Geophys. Space Phys.* **13**, 401–418.

Carslaw, H.S., Jaeger, J.C., 1986. *Conduction of heat in solids*. Oxford University Press, Oxford, MA, 510 p.

Chamberlain, P.C., Ferry, J.M., Rumble III, D., 1990. The effects of net-transfer reactions on the isotopic composition of minerals. *Contrib. Mineral. Petrol.* **105**, 322–336.

Clayton, R.N., Mayeda, T.K., 1963. The use of bromine pentaflouride in the extraction of oxygen from oxides and silicates fro isotopic analysis. *Geochim. Cosmochim. Acta* **27**, 43–52.

Clayton, R.N., Goldsmith, J.R., Mayeda, T.K., 1989. Oxygen isotope fractionation in quartz, albite, anorthite, and calcite. *Geochim. Cosmochim. Acta* **53**, 725–733.

Chiba, H., Chacko, T., Clayton, R.N., Goldsmith, J.R., 1989. Oxygen isotope fractionation involving diopside, forsterite, and calcite: applications to geothermometry. *Geochim. Cosmochim. Acta* **53**, 2985–2995.

DePaolo, D.J., 1981. Trace element and isotopic effects of combined wall rock assimilation and fractional crystallization. *Earth Planet. Sci. Lett.* **53**, 189–202.

Eiler, J.M., Valley, J.W., Baumgartner, L.P., 1993. A new look at stable isotope thermometry. *Geochim. Cosmochim. Acta* **57**, 2571–2583.

Evans-Lamswood, D.M., Butt, D.P., Jackson, R.S., Lee, D.V., Muggridge, M.G., Wheeler, R.I., Wilton, D.H.C., 2000. Physical controls associated with the distribution of sulfides in the Voisey's Bay Ni–Cu–Co Deposit, Labrador. *Econ. Geol.* **95**, 749–769.

Grinenko, L.N., 1985. Sources of sulfur of the nickeliferous and barren gabbro-dolerite intrusions of the northwest Siberian platform. *Intl. Geol. Rev.* **28**, 695–708.

Hamilton, M.A., Emslie, R.F., Roddick, J.C. (1994). Detailed emplacement chronology of basic magmas of the Mid-Proterozoic Nain Plutonic Suite, Labrador: insights from U–Pb systematics in zircon and baddeleyite. Eighth International Conference on Cosmochronology and Isotope Geology. United States Geological Survey Circular 1107, p. 124.

Harris, M., Le Roex, A., Class, C., 2004. Geochemistry of the Uintjiesberg kimberlite, South Africa: petrogenesis of an off-craton, group I, kimberlite. *Lithos* **74**, 149–165.

Halama, R., Marks, M., Brugmann, G., Siebel, W., Wenzel, T., Mark11, G., 2004. Crustal contamination of mafic magmas: evidence from a petrological, geochemical and Sr–Nd–Os–O isotopic study of the Proterozoic Isortoq dike swarm, South Greenland. *Lithos* **74**, 199–232.

Irvine, T.N., 1975. Crystallization sequence of the Muskox Intrusion and other layered intrusions: II. Origin of the chromitite layers and similar deposits of other magmatic ores. *Geochim. Cosmochim. Acta* **39**, 991–1020.

Jenkin, G.R.T., Linklater, C., Fallick, A.E., 1991. Modeling of mineral $\delta^{18}O$ values in an igneous aureole; closed system model predicts apparent open system $\delta^{18}O$ values. *Geology* **19**, 1185–1188.

Lambert, D.D., Foster, J.G., Frick, L.R., Li, C., Naldrett, A.J., 1999. Re–Os isotopic systematics of the Voisey's Bay Ni–Cu–Co magmatic ore system, Labrador, Canada. *Lithos* **47**, 67–88.

Lambert, D.D., Frick, L.R., Foster, J.G., Li, C., Naldrett, A.J., 2000. Re–Os isotope systematics of the Voisey's Bay Ni–Cu–Co magmatic sulfide system, Labrador, Canada: II. Implications for parental magma chemistry, ore genesis, and metal redistribution. *Econ. Geol.* **95**, 867–888.

Lesher, M.C., Burnham, O.M. (1999). Mass balance and mixing in magmatic sulphide systems. In: Keays, R.R., Lesher, C.M., Lightfoot, P.C., Farrow, C.F.G. (Eds.), *Dynamic Processes in Magmatic Ore Deposits and Their Application to Mineral Exploration*, Geol. Assoc. Canada Short Courses Notes, Ottawa, Canada, **13**, pp. 413–449.

Lee, D. (1987). Geothermobarometry and petrologic history of a contact metamorphosed section of the Tasiuyak Gneiss, west of Nain, Labrador. Bachelor of Science (Honors). Memorial University of Newfoundland, St. John's NF.

Li, C., Naldrett, A.J., 1993. Sulfide capacity of magma: a quantitative model and its application to the formation of sulfide ores at Sudbury, Ontario. *Econ. Geol.* **88**, 1253–1260.

Li, C., Naldrett, A.J., 1999. Geology and petrology of the Voisey's Bay intrusion: reaction of olivine with sulfide and silicate liquids. *Lithos* **47**, 1–31.

Li, C., Naldrett, A.J., 2000. Melting reactions of gneissic inclusions with enclosing magma at Voisey's Bay, Labrador, Canada: implications with respect to ore genesis. *Econ. Geol.* **95**, 801–814.

Li, C., Ripley, E.M., 2005. Empirical equations to predict the sulfur content of mafic magmas at sulfide saturation and applications to magmatic sulfide deposits. *Mineralium Deposita* **40**, 218–230.

Mariga, J., Ripley, E.M., Li, C., 2006. Petrogenetic evolution of gneissic xenoliths in the Voisey's Bay Intrusion, Labrador, Canada: mineralogy, reactions, partial-melting and mechanisms of mass transfer. *Geochemistry, Geophysics, Geosystems*, Q05013. doi:10.1029/2005GC001184.

McFarlane, C.R.M., Carlson, W.D., Connelly, J.N., 2003. Prograde, peak, and retrograde P–T paths from aluminum in orthopyroxene: high-temperature contact metamorphism in the aureole of the Makhavinekh Lake Pluton, Nain Plutonic Suite, Labrador. *J. Metamorphic Geol.* **21**, 405–423.

Naldrett, A.J., Keats, H., Spakes, K., Moore, R., 1996. Geology of the Voisey's Bay Ni–Cu–Co deposit, Labrador, Canada. *Exploration and Mining Geol.* **5**, 169–179.

Naldrett, A.J., 1999. World class Ni–Cu–PGE deposits: key factors in their genesis. *Mineralium Deposita* **34**, 227–240.

Ripley, E.M. (1999). Systematics of sulphur and oxygen isotopes in mafic igneous rocks and related Cu–Ni–PGE mineralization. In: Keays, R.R., Lesher, C.M., Lightfoot, P.C., Farrow, C.F.G. (Eds.), *Dynamic Processes in Magmatic Ore Deposits and Their Application to Mineral Exploration*, Geol. Assoc. Canada Short Courses Notes, Ottawa, Canada **13**, pp. 133–158.

Ripley, E.M., Park, Y.R., Li, C., Naldrett, A.J., 1999. Sulfur and oxygen isotopic evidence of country rock contamination in the Voisey's Bay Ni–Cu–Co deposit, Labrador, Canada. *Lithos* **47**, 53–68.

Ripley, E.M., Park, Y.R., Naldrett, A.J., Li, C., 2000. Oxygen isotopic studies of the Voisey's Bay Ni–Cu–Co deposit, Labrador, Canada. *Econ. Geol.* **95**, 831–844.

Ripley, E.M., Li, C., Shin, D., 2002. Gneiss assimilation in the genesis of magmatic Ni–Cu–Co sulfide mineralization at Voisey's Bay, Labrador: $\delta^{34}S$, $\delta^{13}C$, and Se/S evidence. *Econ. Geol.* **97**, 1307–1318.

Rumble III, D., Spear, F.S., 1983. Oxygen-isotopic equilibration and permeability enhancement during regional metamorphism. *J. Geol. Soc. London* **140**, 619–628.

Ryan, B., 2000. The Nain-Churchill boundary and the Nain Plutonic Suite: a regional perspective on the geologic setting of the Voisey's Bay Ni–Cu–Co deposit. *Econ. Geol.* **95**, 703–724.

Ryan, B., Wardle, R.J., Gower, C., Nunn, G.G. (1995). Nickel-copper sulfide mineralization in Labrador: The Voisey's Bay discovery and its exploration implications. Current Research Newfoundland Department of Natural Resources, Geological Survey, Report 95-1,177-204.

Schiffries, C.M., Rye, D.M., 1989. Stable isotope systematics of the Bushveld Complex: I. Constrains of magmatic processes in layered intrusions. *Amer. J. Sci.* **289**, 841–873.

Sharp, Z.D., Atudorei, V., Durakiewiez, T., 2001. A rapid method for determination of hydrogen and oxygen isotope ratio from water and hydrous minerals. *Chem. Geol.* **173**, 197–210.

Sharp, Z.D., 1995. Oxygen isotope geochemistry of the Al_2SiO_5 polymorphs. *Amer. J. Sci.* **295**, 1058–1076.

Sparks, R.J S., 1986. The role of crustal contamination in magma evolution through geologic time. *Earth Planet. Sci. Lett.* **78**, 211–223.

Spera, F.J., Bohrson, W.A., 2001. Energy-constrained open system magmatic processes I: general model and energy constrained assimilation and fractional crystallization (EC-AFC) formulation. *J. Petrol.* **42**, 999–1018.

Taylor Jr., H.P., 1980. The effects of assimilation of country rocks by magma on $^{18}O/^{16}O$ and $^{87}Sr/^{86}Sr$ systematics in igneous rocks. *Earth Planet. Sci. Lett.* **47**, 243–254.

Wardle, R.J. (1983). Nain-Churchill province cross-section, Nachvak Fiord, northern Labrador. Newfoundland Department of Mines and

Energy, Mineral Development Division, Current Research Report, 83-1, 68-90.

Wardle, R.J., Ryan, A.B., Philippe, S., and Scharer, U. (1990a). Proterozoic crustal development, Goose Bay region, Grenville Province, Labrador, Canada. In: Gower, C.F., Rivers, T., Ryan, B. (Eds.), *Mid-Proterozic Laurentia-Baltica*, Geological Association of Canada, Special Paper **38**, pp. 197–214.

Wardle, R.J., Ryan, A.B., Nunn, G.A.G., Mengel, F.C., 1990b. Labrador segment of the trans-Hudson orogen: crustal development through oblique convergence and collision. *Geol. Assoc. Canada Special Paper* **37**, 353–370.

Zhao, Z.F., Zheng, Y.F., 2003. Calculation of oxygen isotope fractionation in magmatic rocks. *Chem. Geol.* **193**, 59–80.

Zheng, Y.F., 1991. Calculation of oxygen isotope fractionation in metal oxides. *Geochim. Cosmochim. Acta* **55**, 2299–2307.

Zheng, Y.F., 1993. Calculation of oxygen isotope fractionation in anhydrous silicate minerals. *Geochim. Cosmochim. Acta* **57**, 1079–1091.